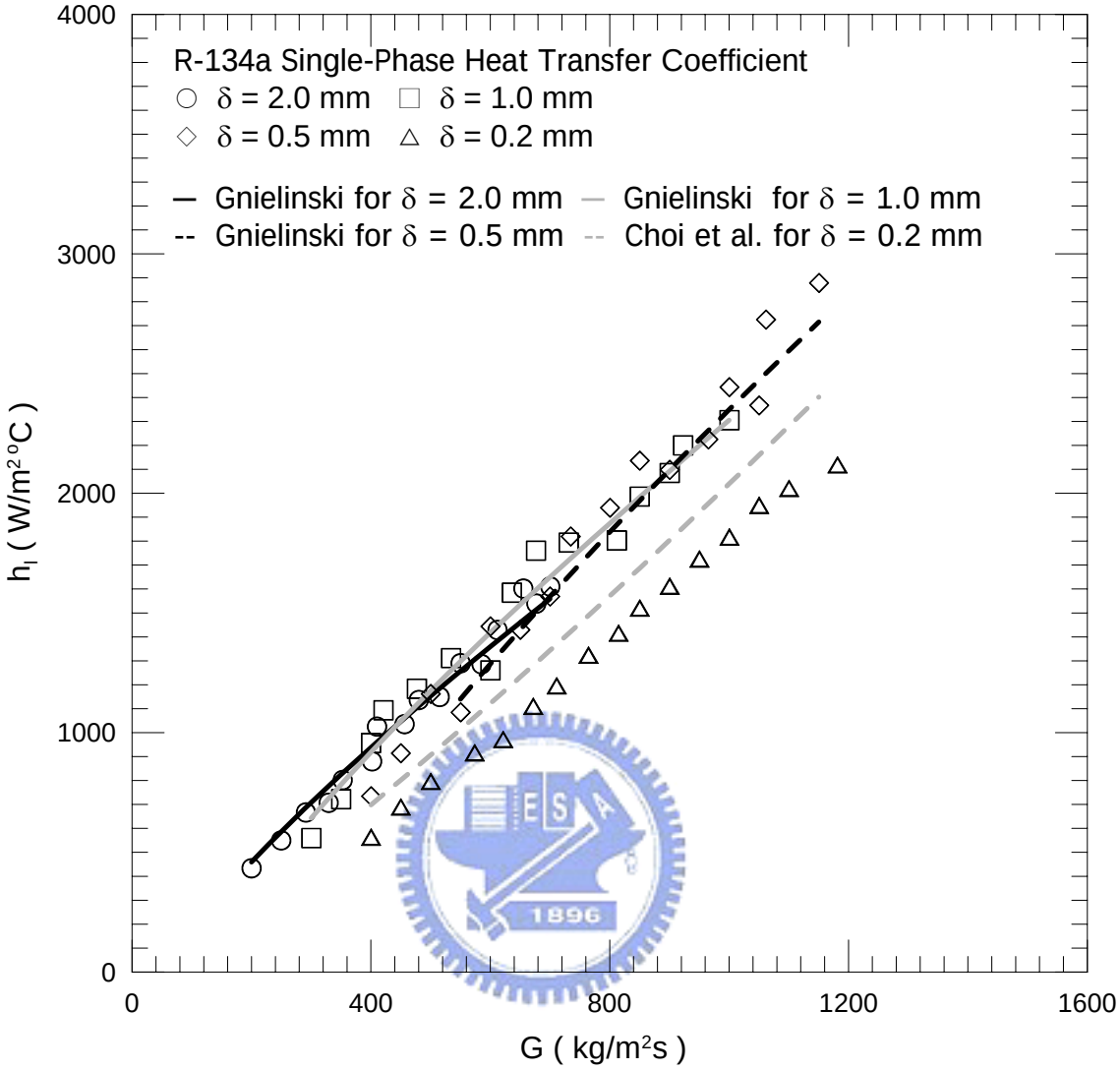

Fig. 4.1 Comparison of the present single-phase liquid convection heat transfer data with the correlation of Gnielinski [70] and Choi et al. [71].

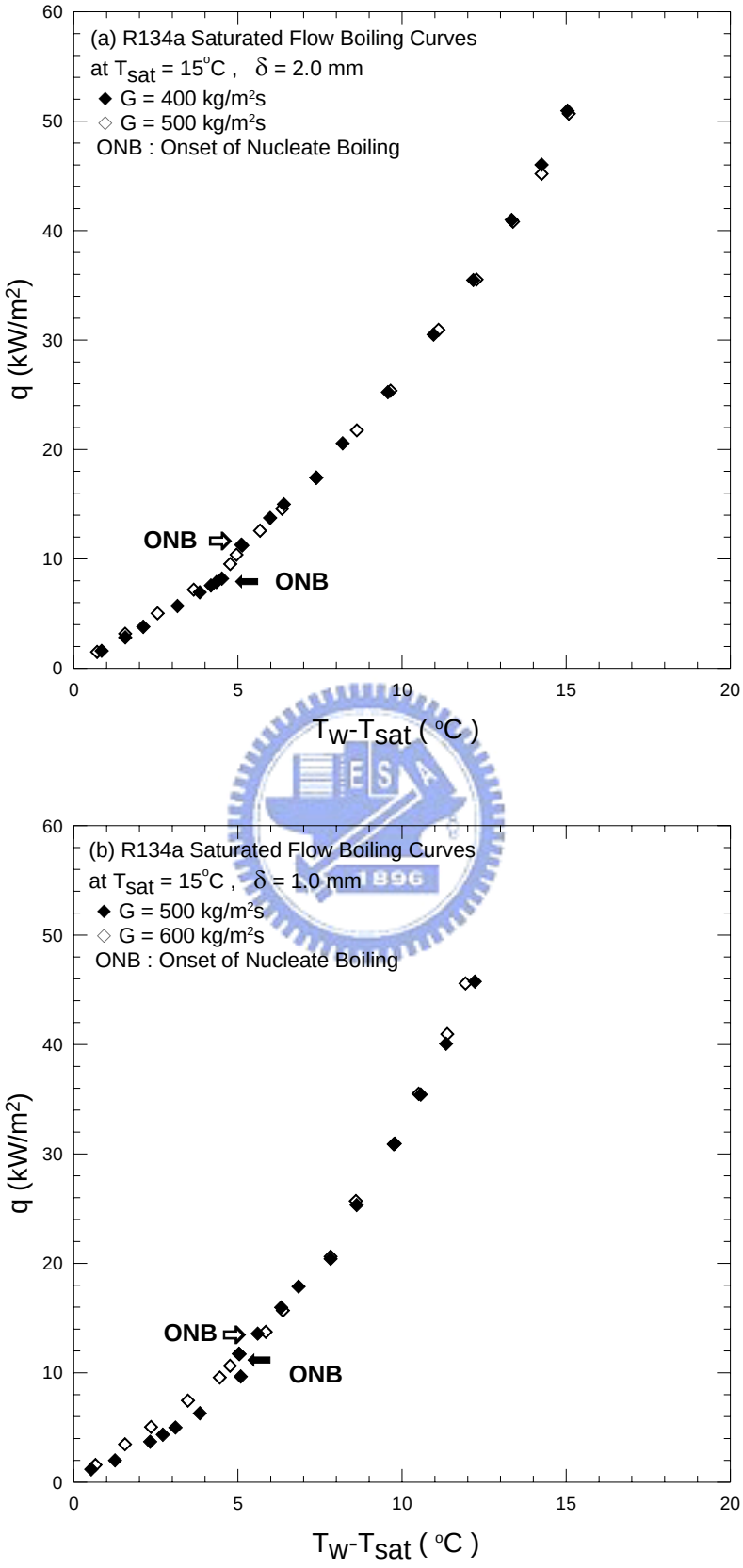

Fig. 4.2 Saturated flow boiling curves for various refrigerant mass fluxes at (a) T_{sat}= 15℃ & δ = 2.0 mm and (b) T_{sat}= 15℃ & δ = 1.0 mm.

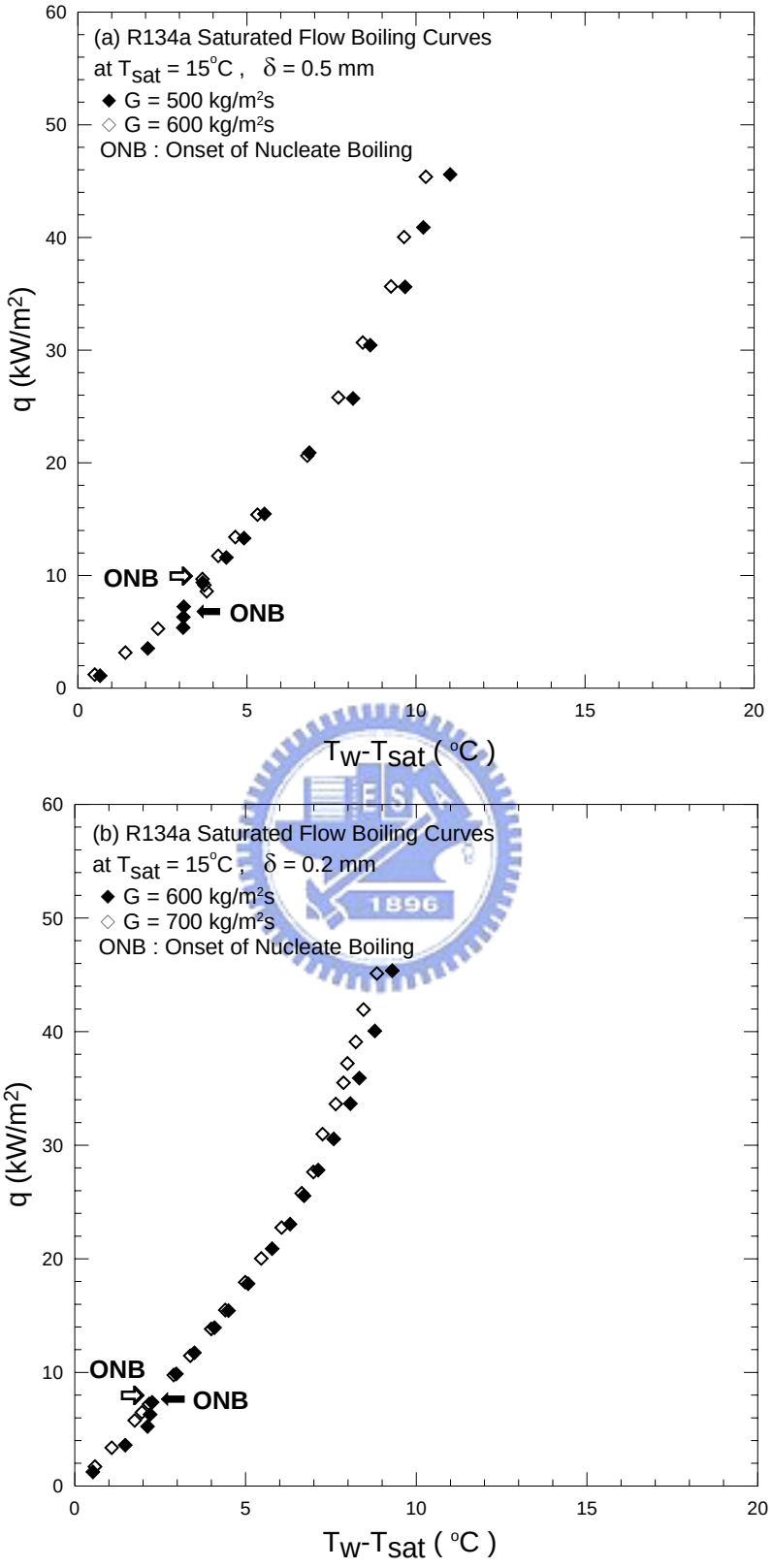

Fig. 4.3 Saturated flow boiling curves for various refrigerant mass fluxes at (a) T_{sat}= 15℃ & δ = 0.5 mm and (b) T_{sat}= 15℃ & δ = 0.2 mm.

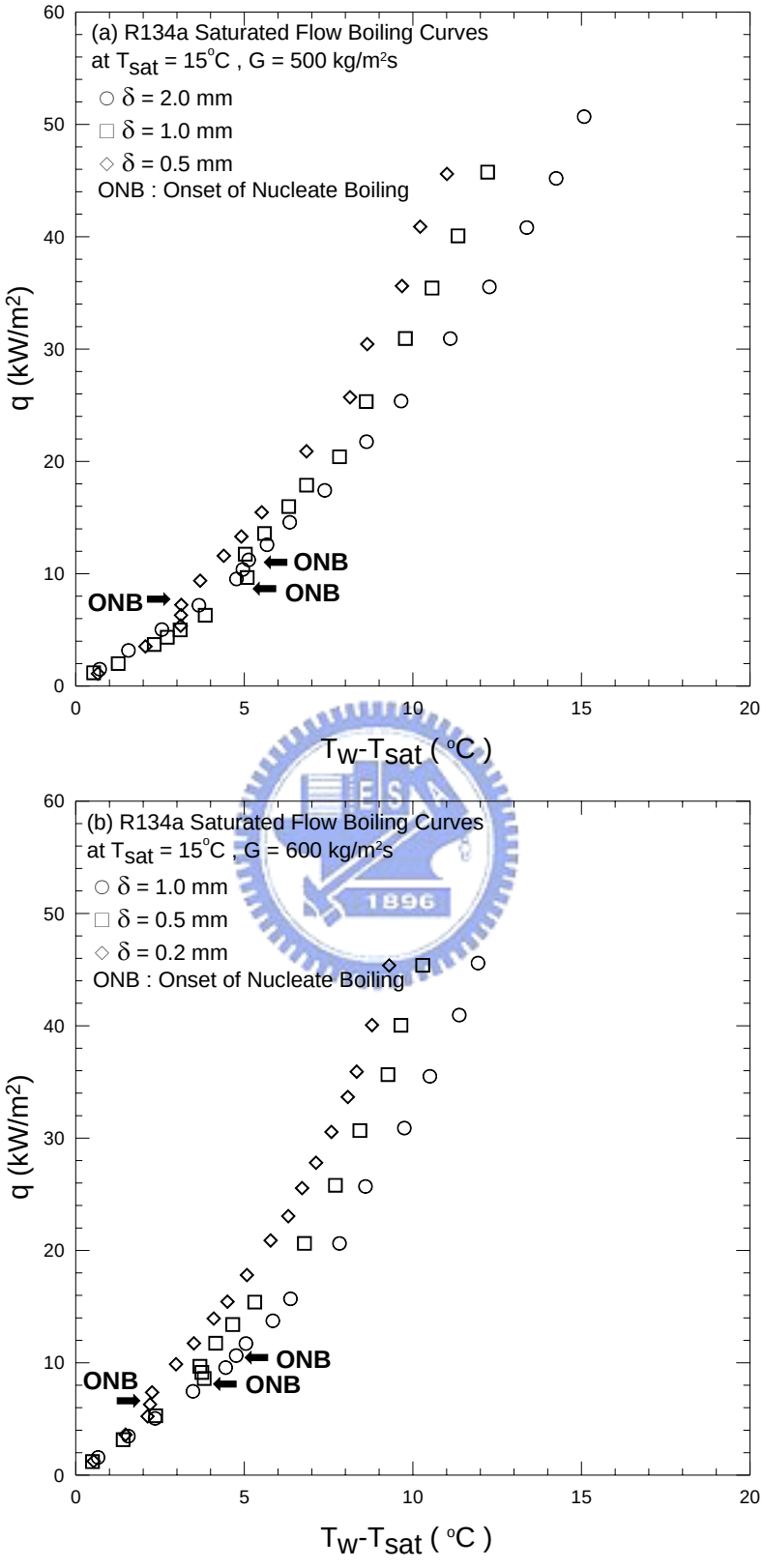

Fig. 4.4 Saturated flow boiling curves for various gap sizes at (a) T_{sat}= 15℃ & G= 500 kg/m^{2}s and (b) T_{sat}= 15℃ & G= 600 kg/m^{2}s.

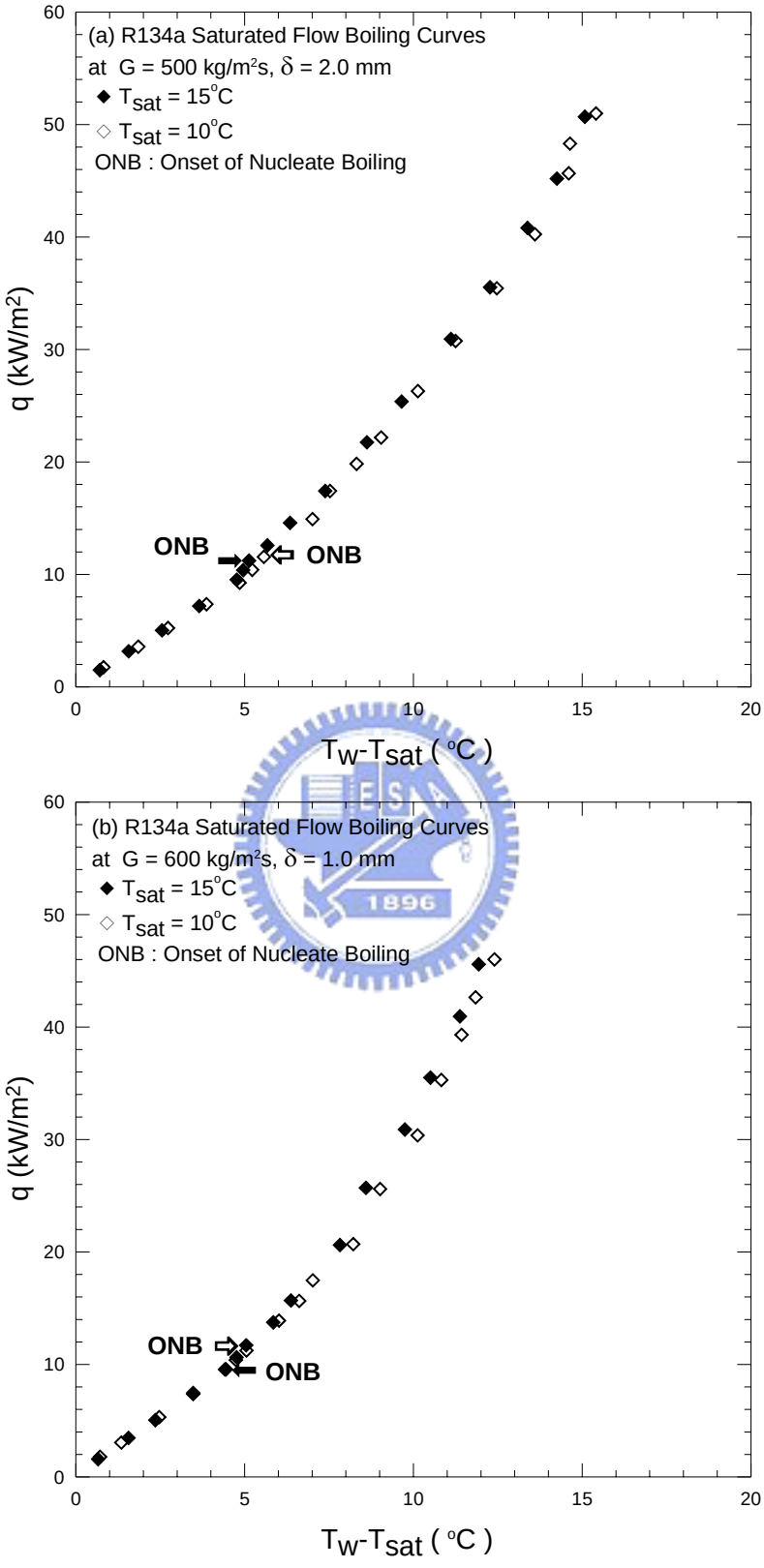

Fig. 4.5 Saturated flow boiling curves for various refrigerant saturated temperatures at (a) G= 500 kg/m^{2}s & δ = 2.0 mm and (b) G= 600 kg/m^{2}s & δ = 1.0 mm.

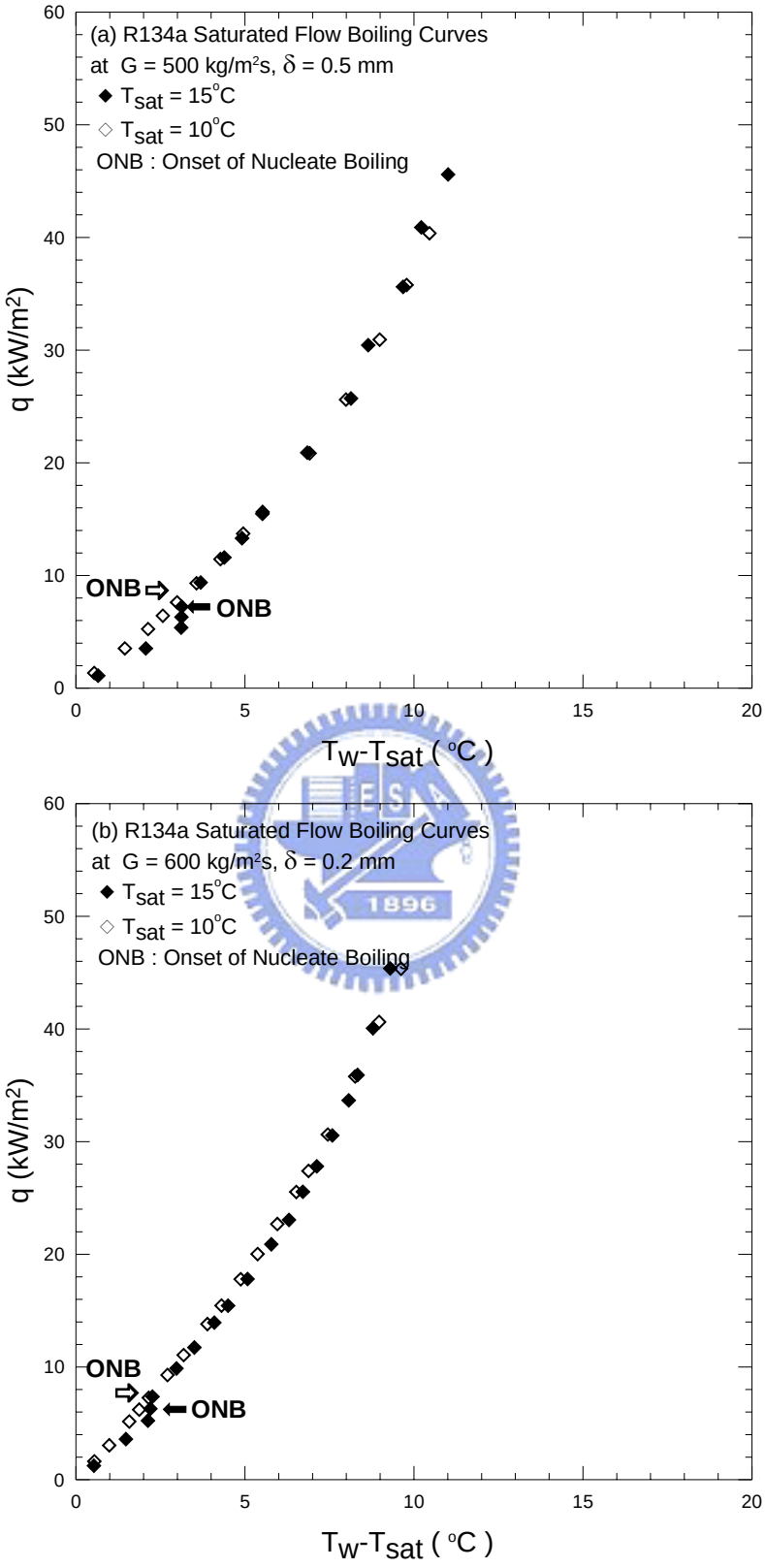

Fig. 4.6 Saturated flow boiling curves for various refrigerant saturated temperatures at (a) G= 500 kg/m^{2}s & δ = 0.5 mm and (b) G= 600 kg/m^{2}s & δ = 0.2 mm.

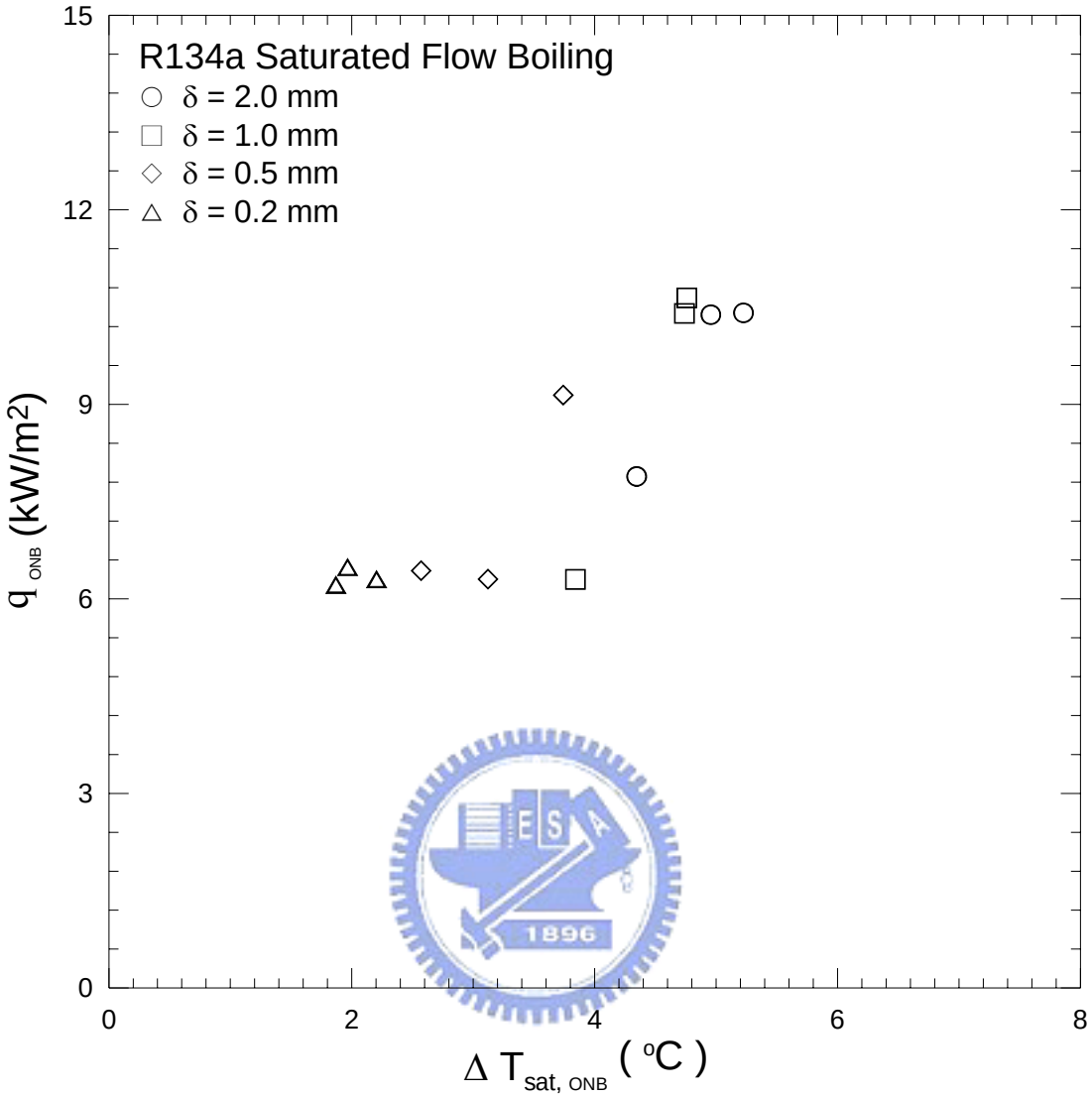

Fig. 4.7 Relation between imposed heat flux and wall superheat at the incipient boiling.

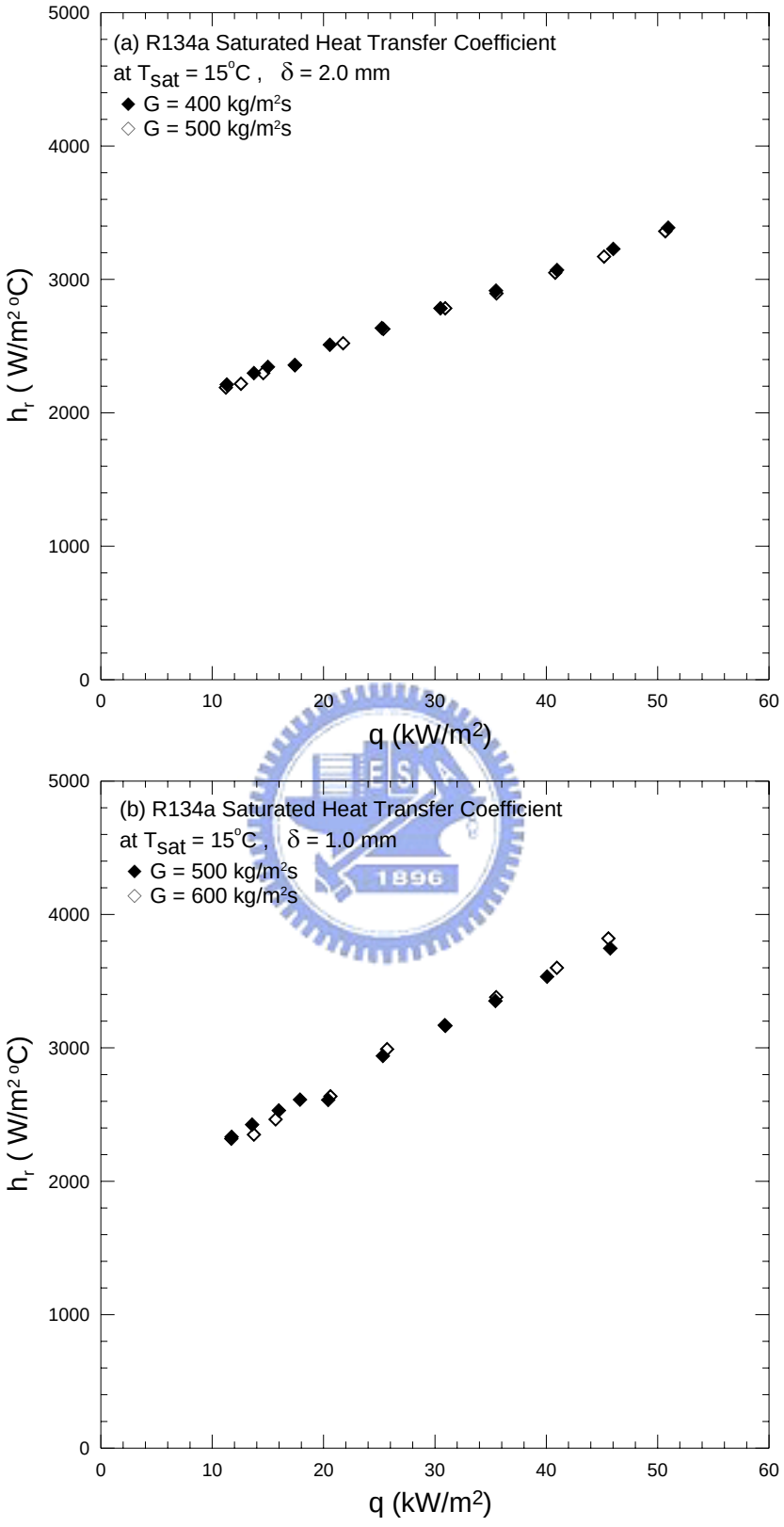

Fig. 4.8 Saturated flow boiling heat transfer coefficient for various refrigerant mass fluxes at (a) T_{sat}= 15℃ & δ = 2.0 mm and (b) T_{sat}= 15℃ & δ = 1.0 mm.

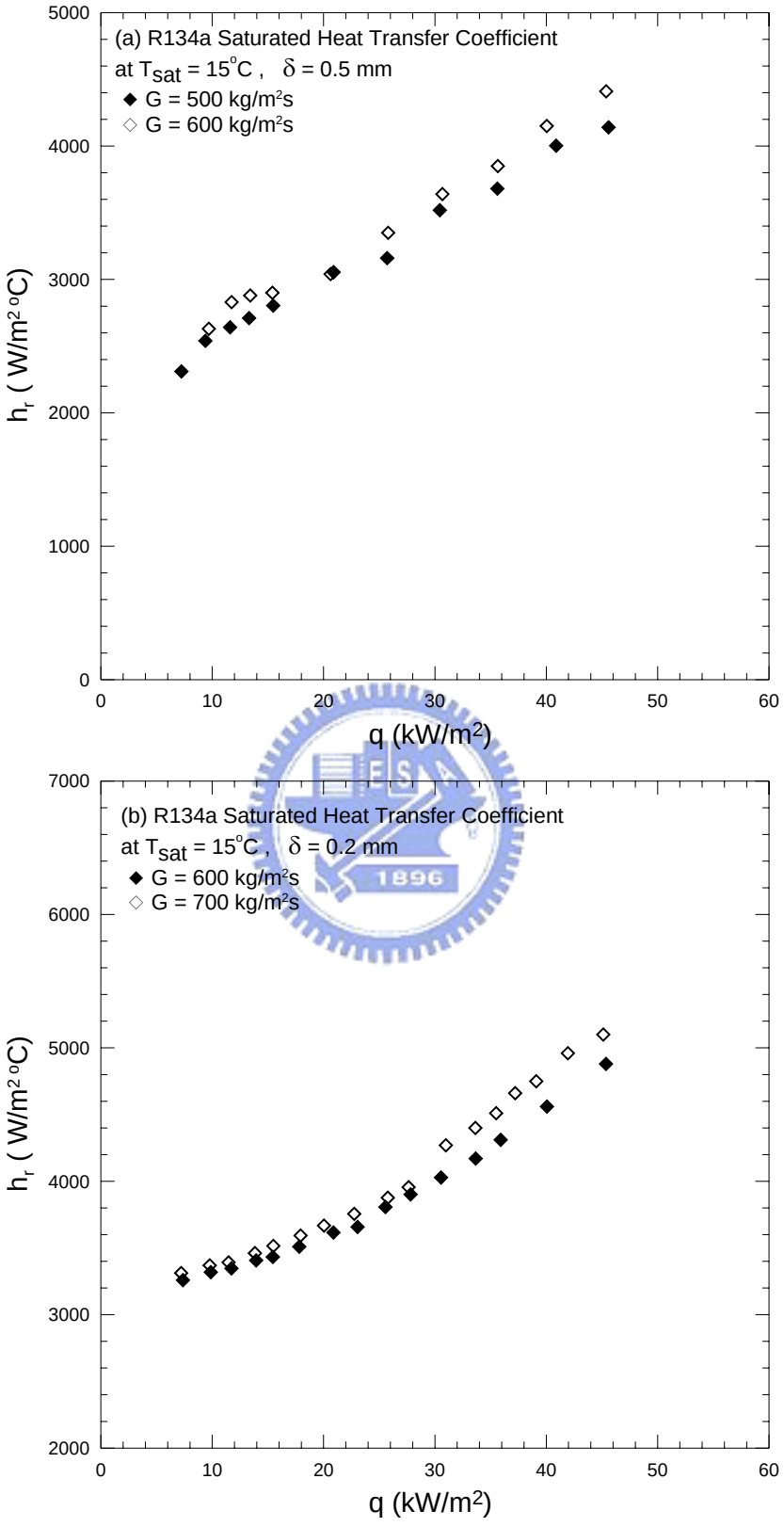

Fig. 4.9 Saturated flow boiling heat transfer coefficient for various refrigerant mass fluxes at (a) T_{sat}= 15℃ & δ = 0.5 mm and (b) T_{sat}= 15℃ & δ = 0.2 mm.

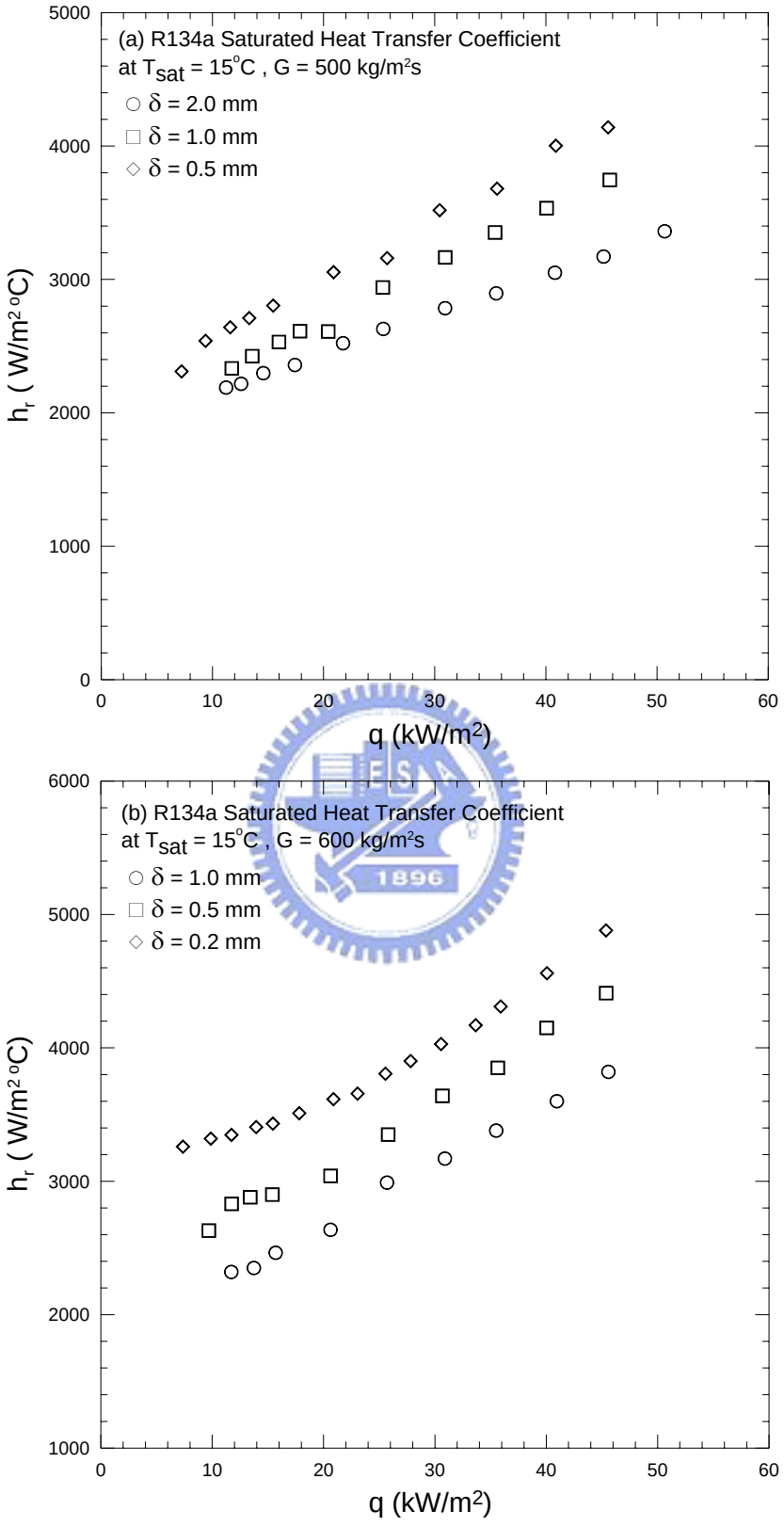

Fig. 4.10 Saturated flow boiling heat transfer coefficient for various gap sizes at (a) T_{sat}= 15℃ & G= 500 kg/m^{2}s and (b) T_{sat}= 15℃ & G= 600 kg/m^{2}s.

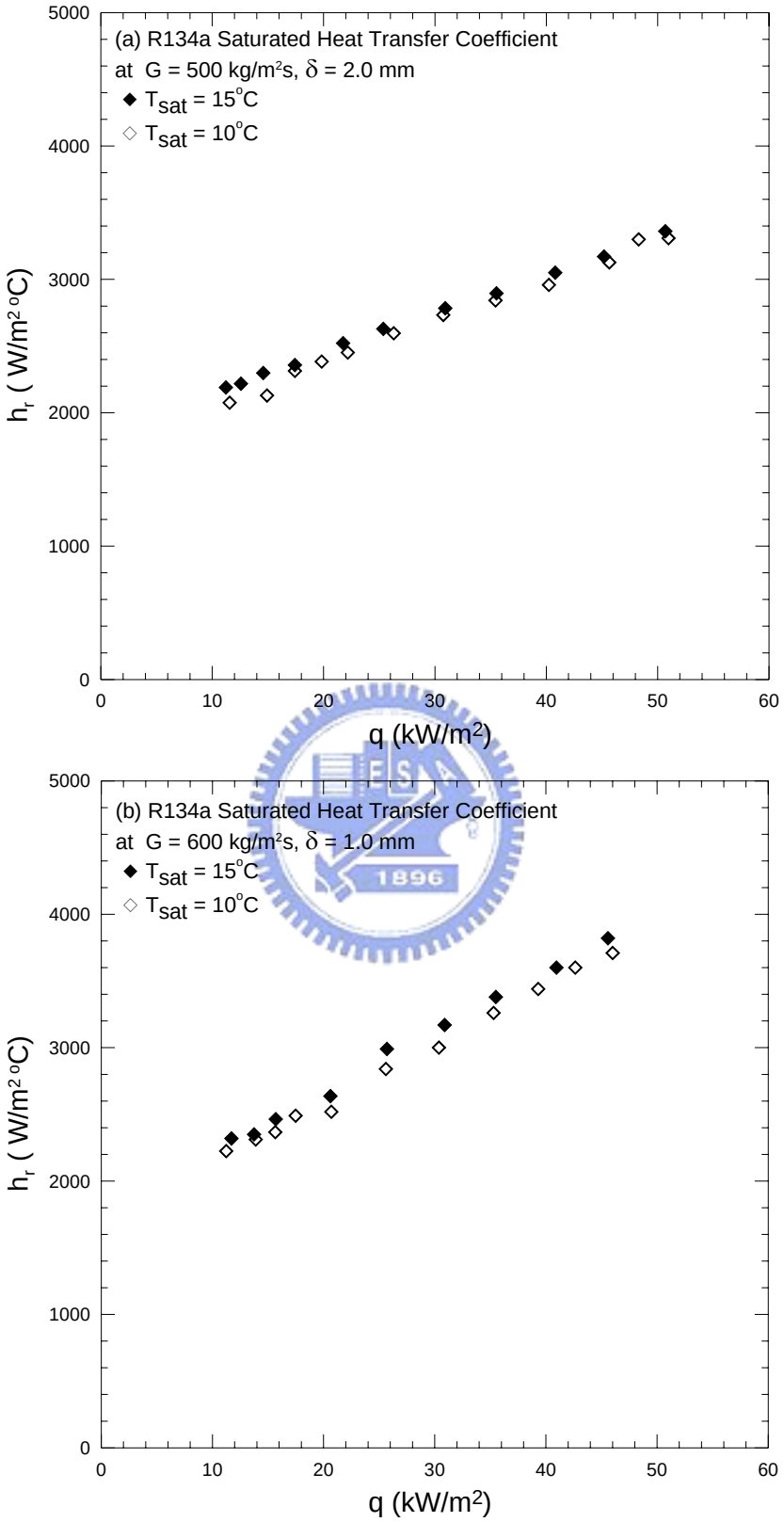

Fig. 4.11 Saturated flow boiling heat transfer coefficient for various refrigerant saturated temperatures at (a) G= 500 kg/m^{2}s & δ = 2.0 mm and (b) G= 600 kg/m^{2}s & δ = 1.0 mm.

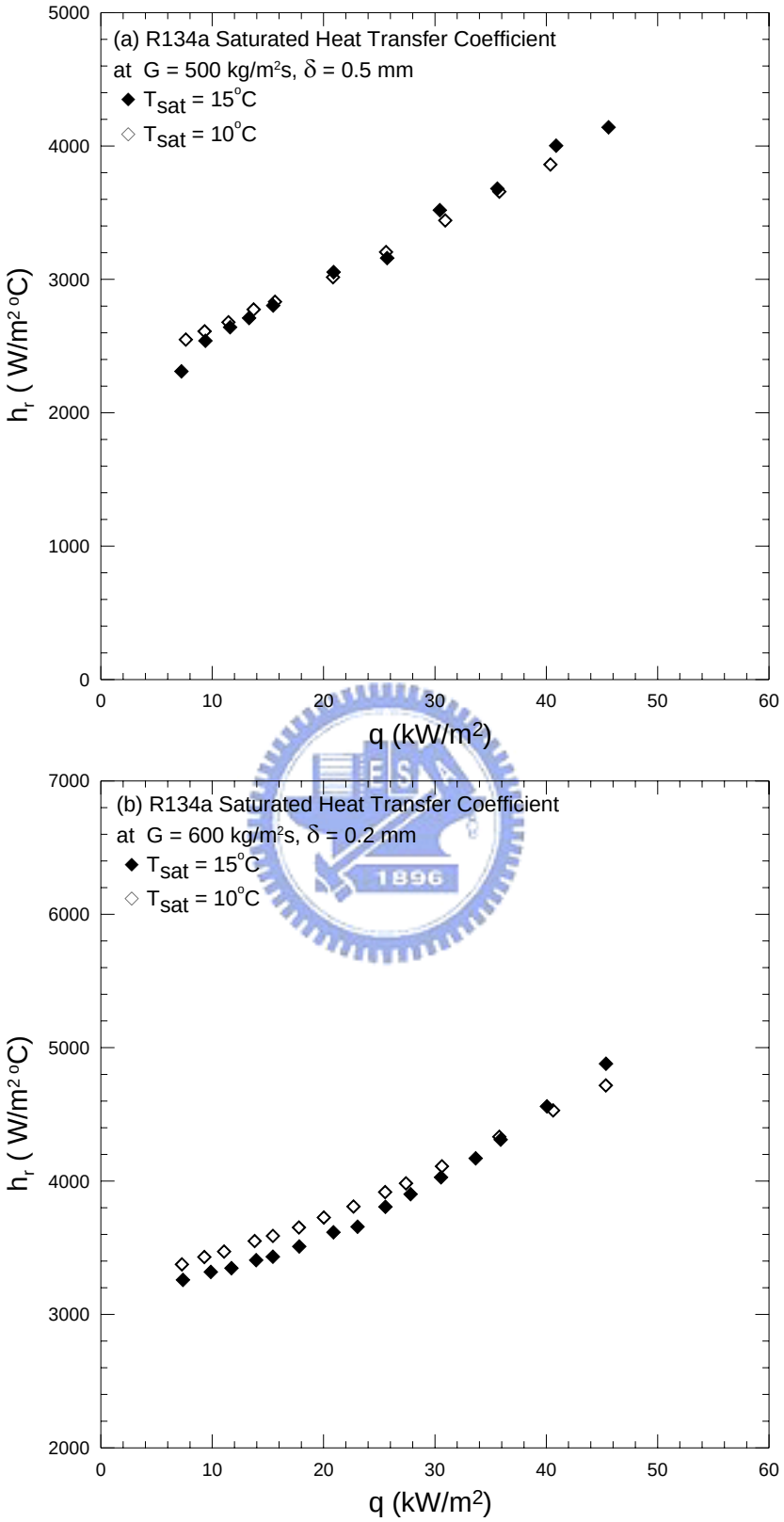

Fig. 4.12 Saturated flow boiling heat transfer coefficient for various refrigerant saturated temperatures at (a) G= 500 kg/m^{2}s & δ = 0.5 mm and (b) G= 600 kg/m^{2}s & δ = 0.2 mm.

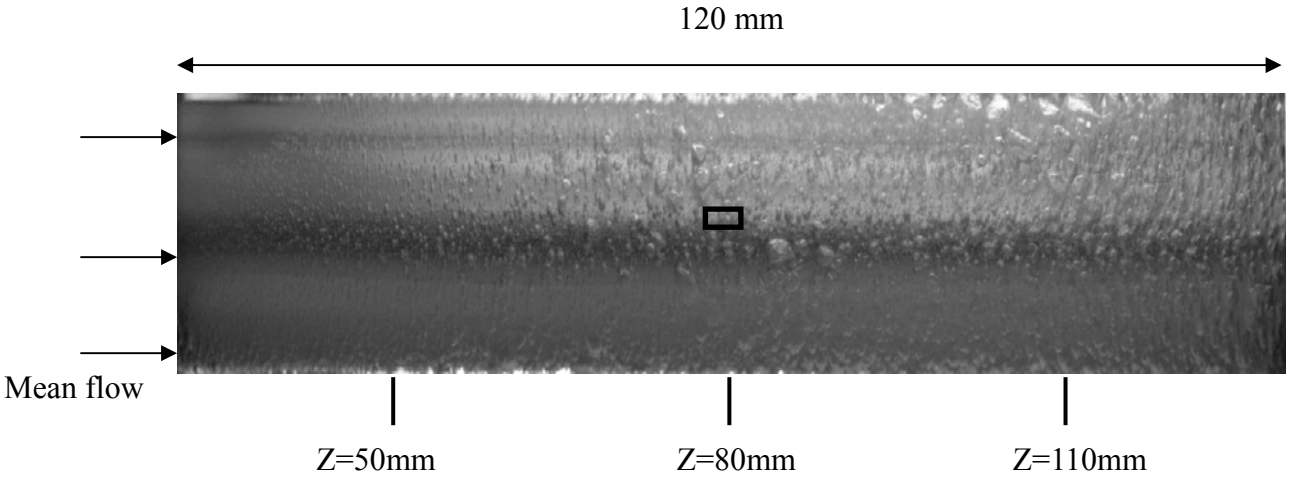

(a)Side view

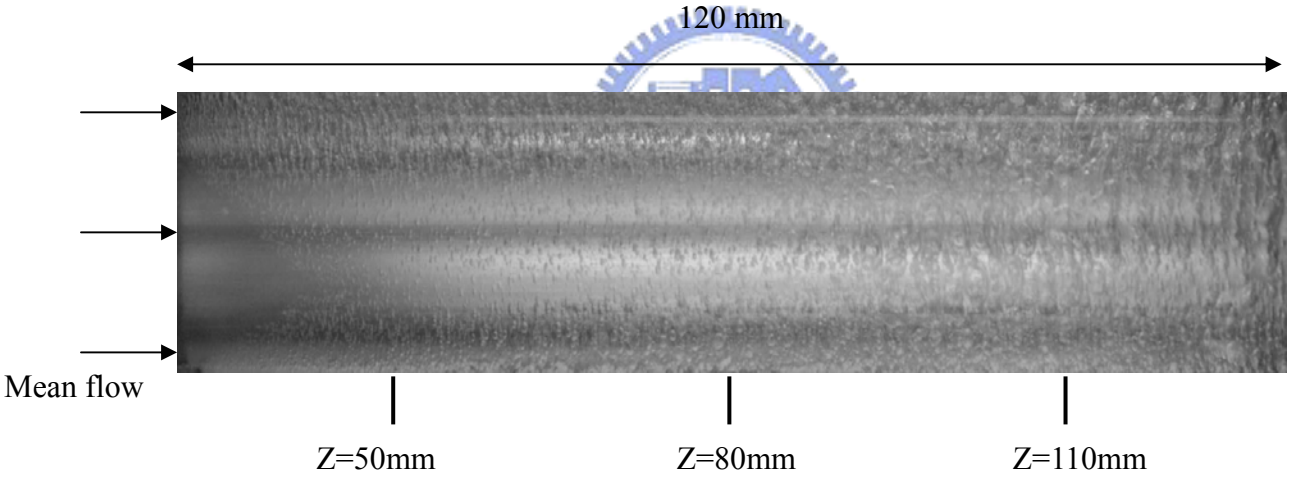

(b) Top view

Fig. 4.13 Photos of boiling flow in the saturated flow boiling of R-134a in the entire duct at G= 500 kg/m^{2}s, T_{sat}= 15℃, δ= 2.0 mm and q= 30 kW/m^2 from (a) side view and (b) top view.

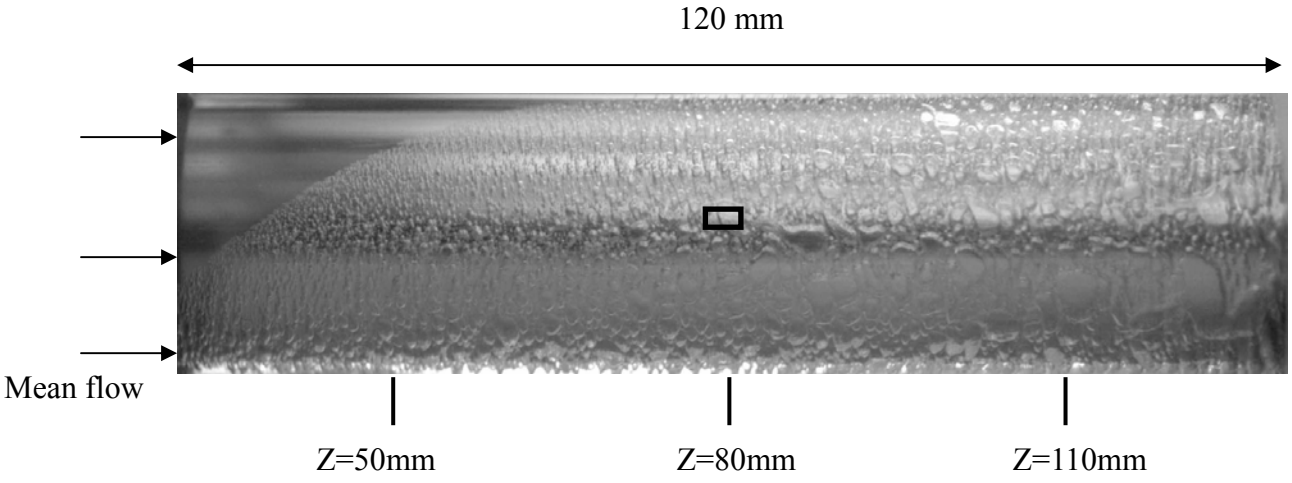

(a)Side view

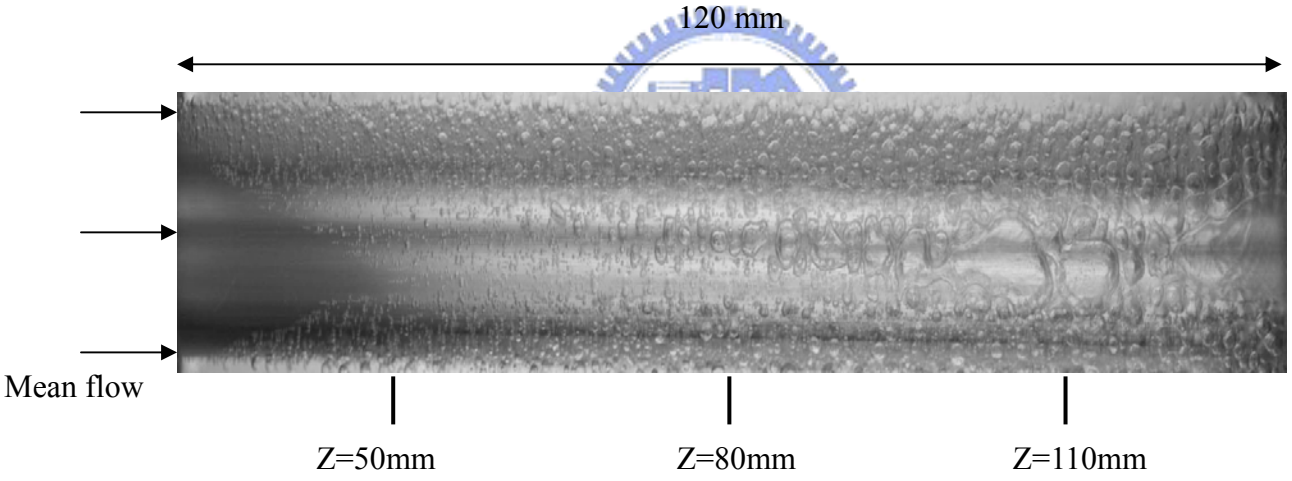

(b) Top view

Fig. 4.14 Photos of boiling flow in the saturated flow boiling of R-134a in the entire duct at G= 600 kg/m^{2}s, T_{sat}= 15℃, δ= 1.0 mm and q= 30 kW/m^2 from (a) side view and (b) top view.

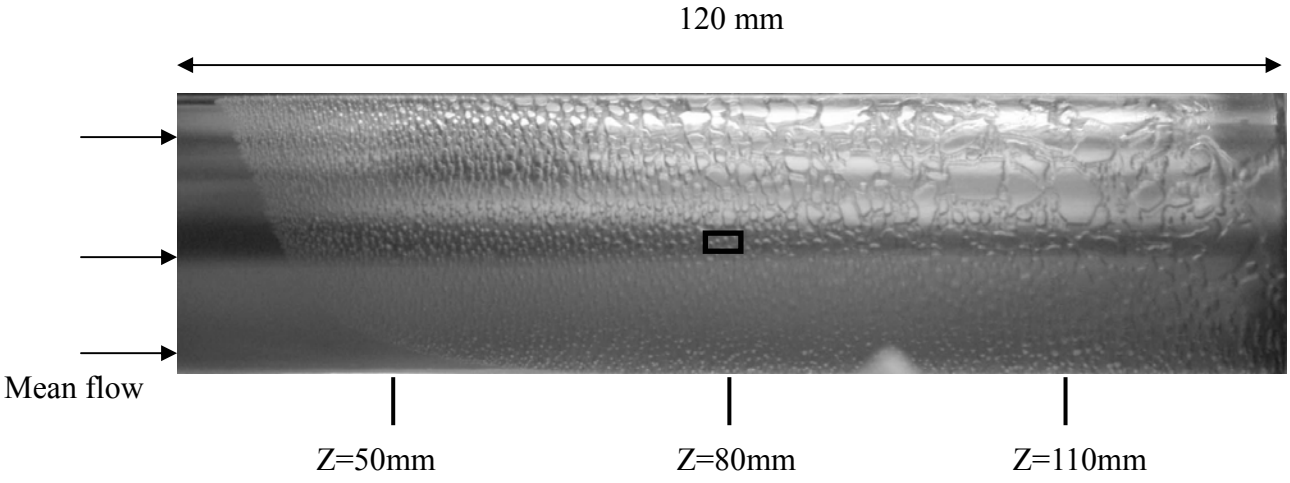

(a)Side view

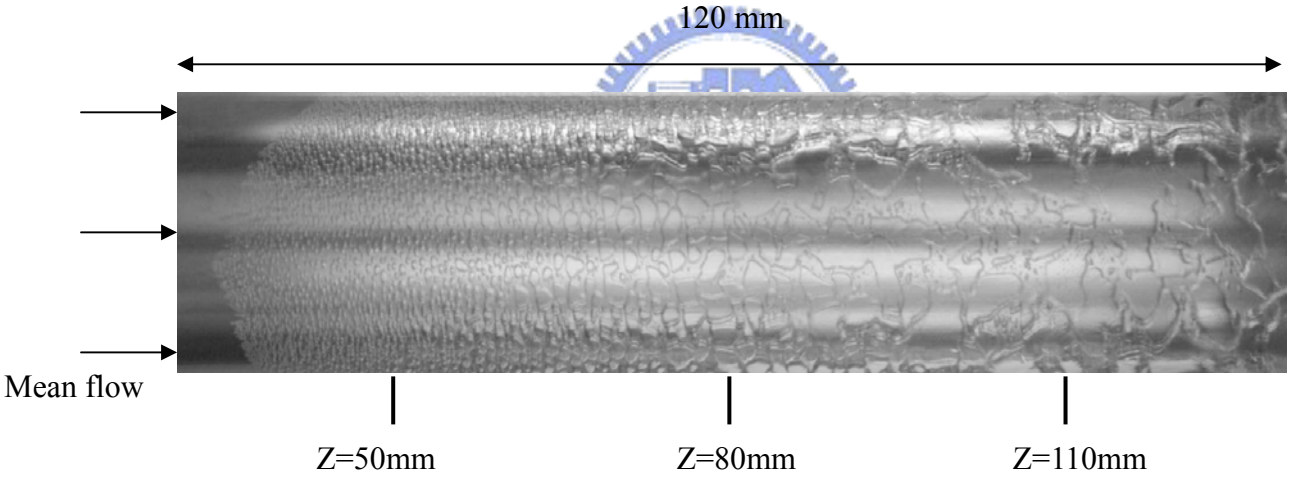

(b) Top view

Fig. 4.15 Photos of boiling flow in the saturated flow boiling of R-134a in the entire duct at G= 600 kg/m^{2}s, T_{sat}= 15℃, δ= 0.5 mm and q= 30 kW/m^2 from (a) side view and (b) top view.

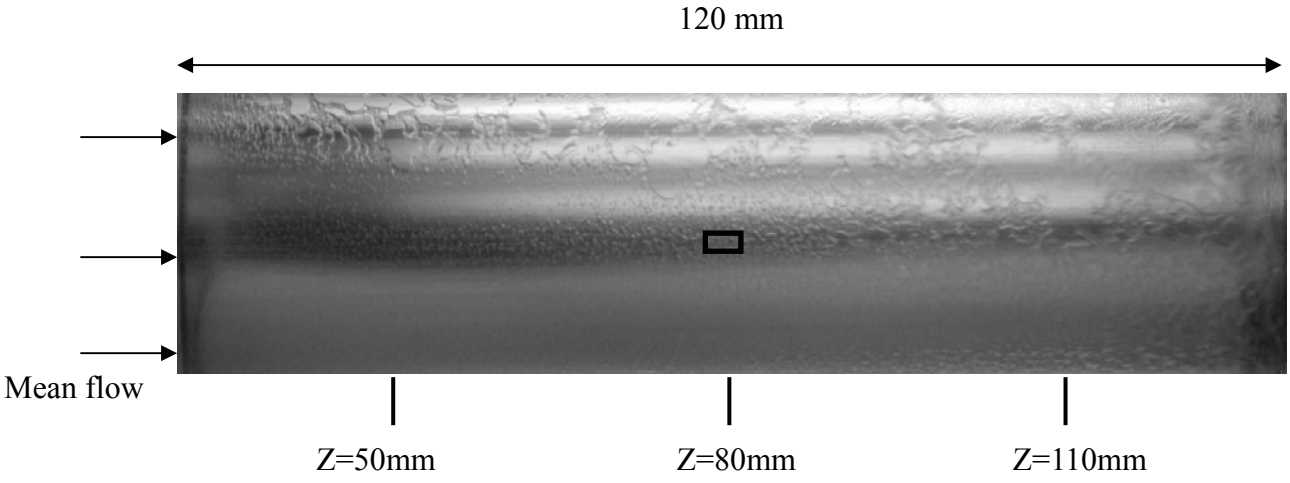

(a)Side view

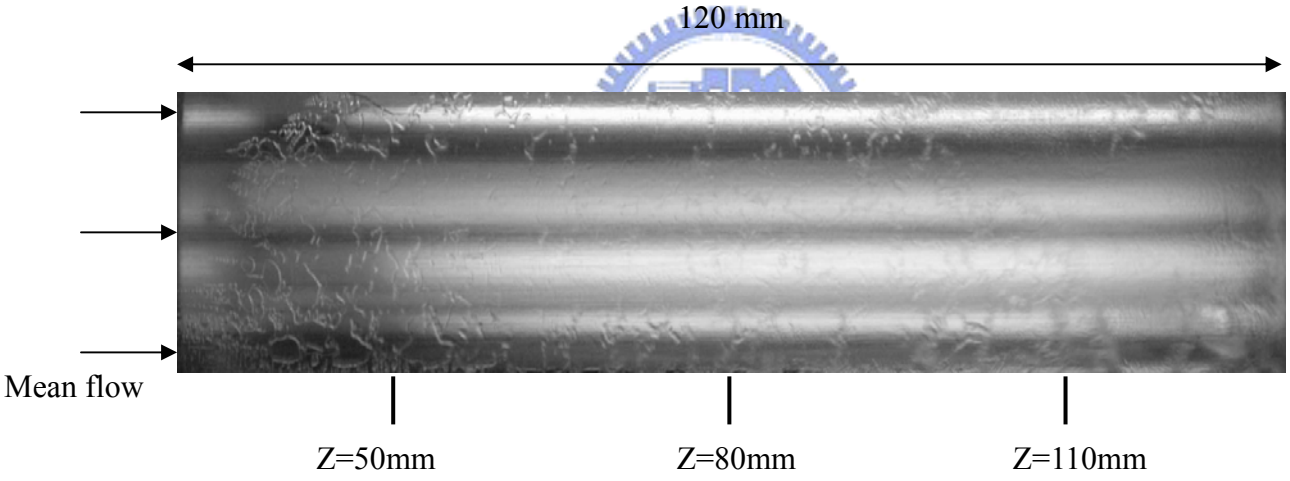

(b) Top view

Fig. 4.16 Photos of boiling flow in the saturated flow boiling of R-134a in the entire duct at G= 600 kg/m^{2}s, T_{sat}= 15℃, δ= 0.2 mm and q=30 kW/m^2 from (a) side view and (b) top view.

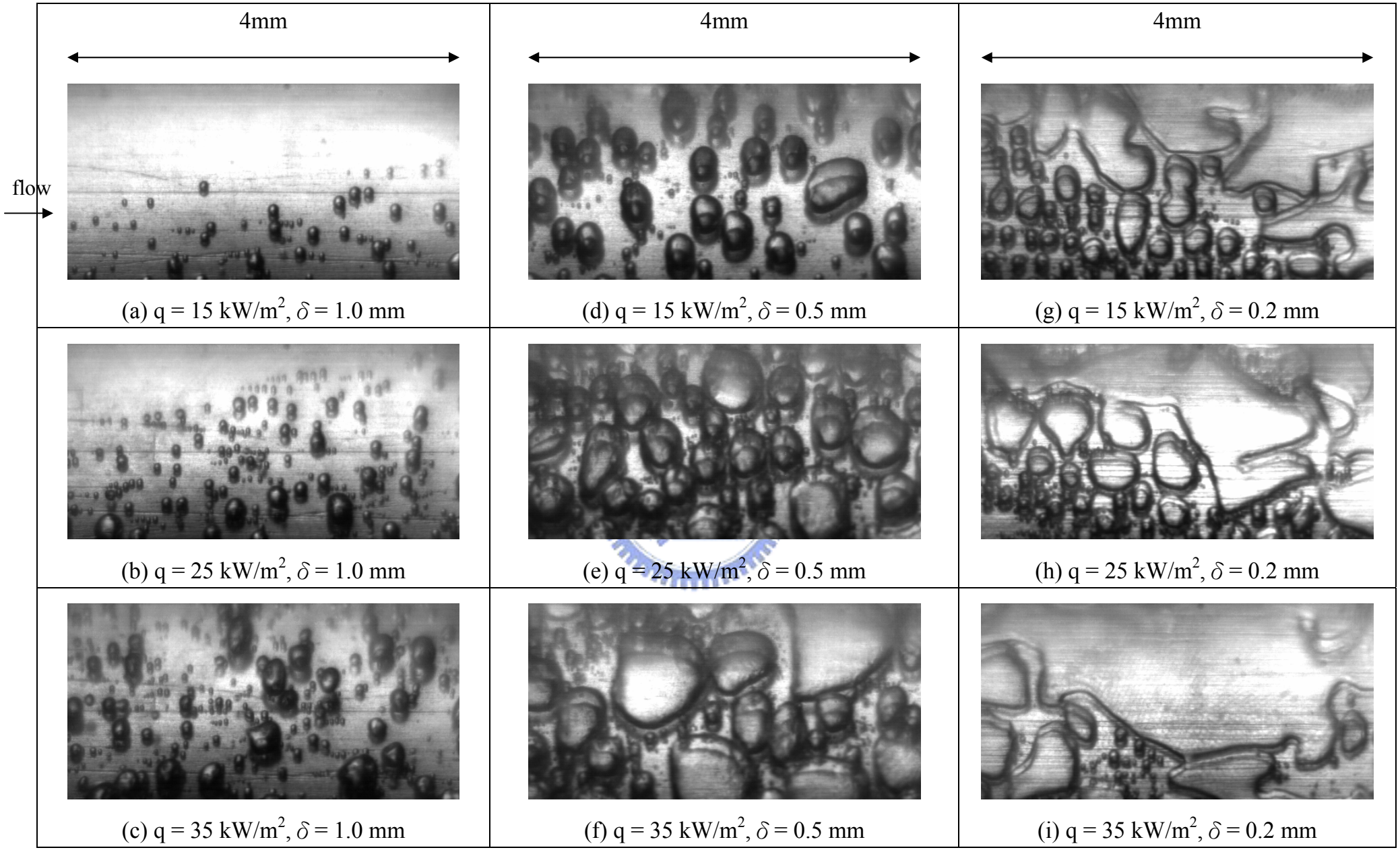

Fig. 4.17 Photos of bubbles in the saturated flow boiling of R-134a in a small region around middle axial location at T_{sat}= 15℃ and G= 600-kg/m^{2}s for various imposed heat flux and gap sizes.

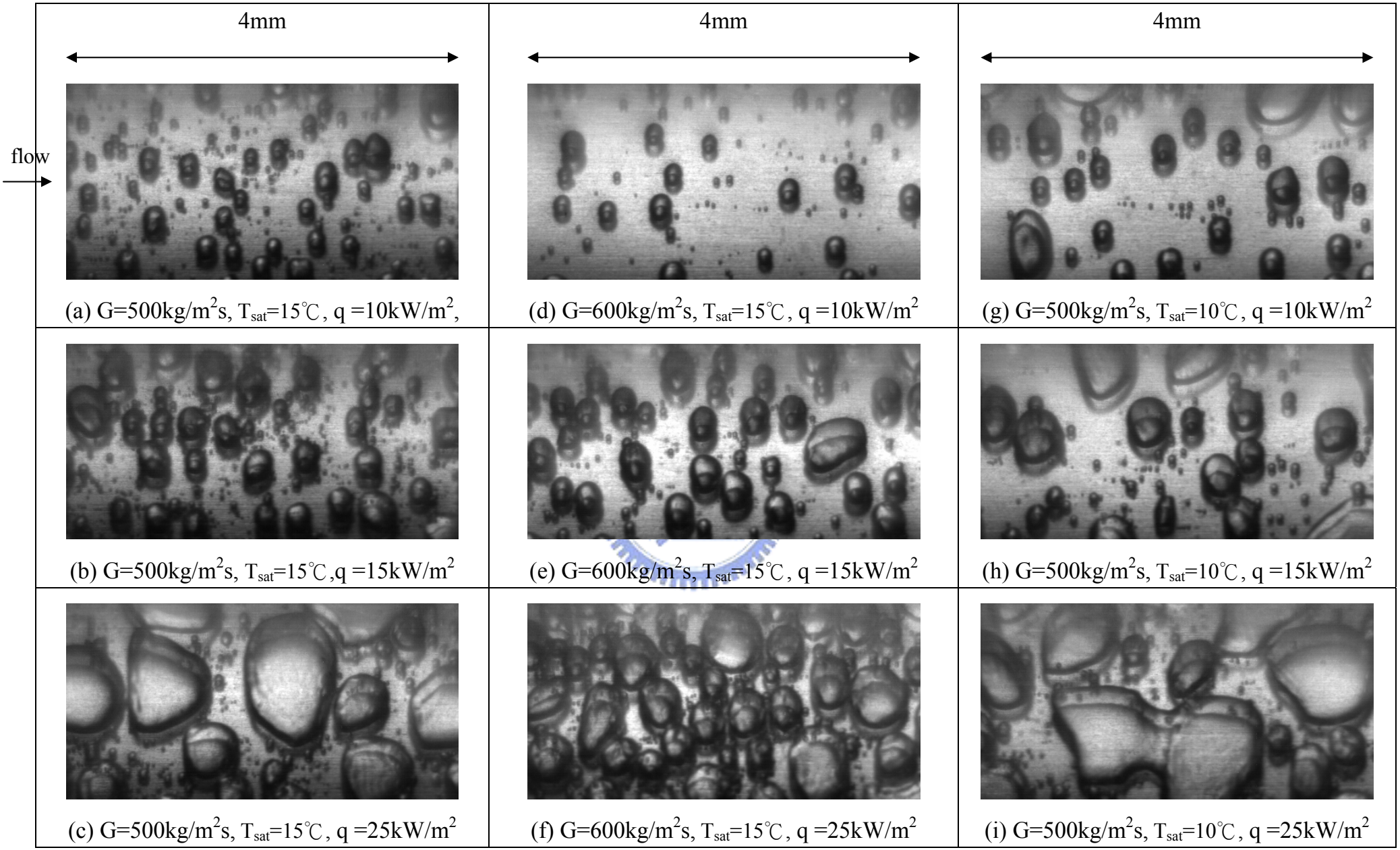

Fig. 4.18 Photos of bubbles in the saturated flow boiling of R-134a in a small region around middle axial location at δ= 0.5 mm for various imposed heat flux, mass fluxes and refrigerant saturated temperatures.

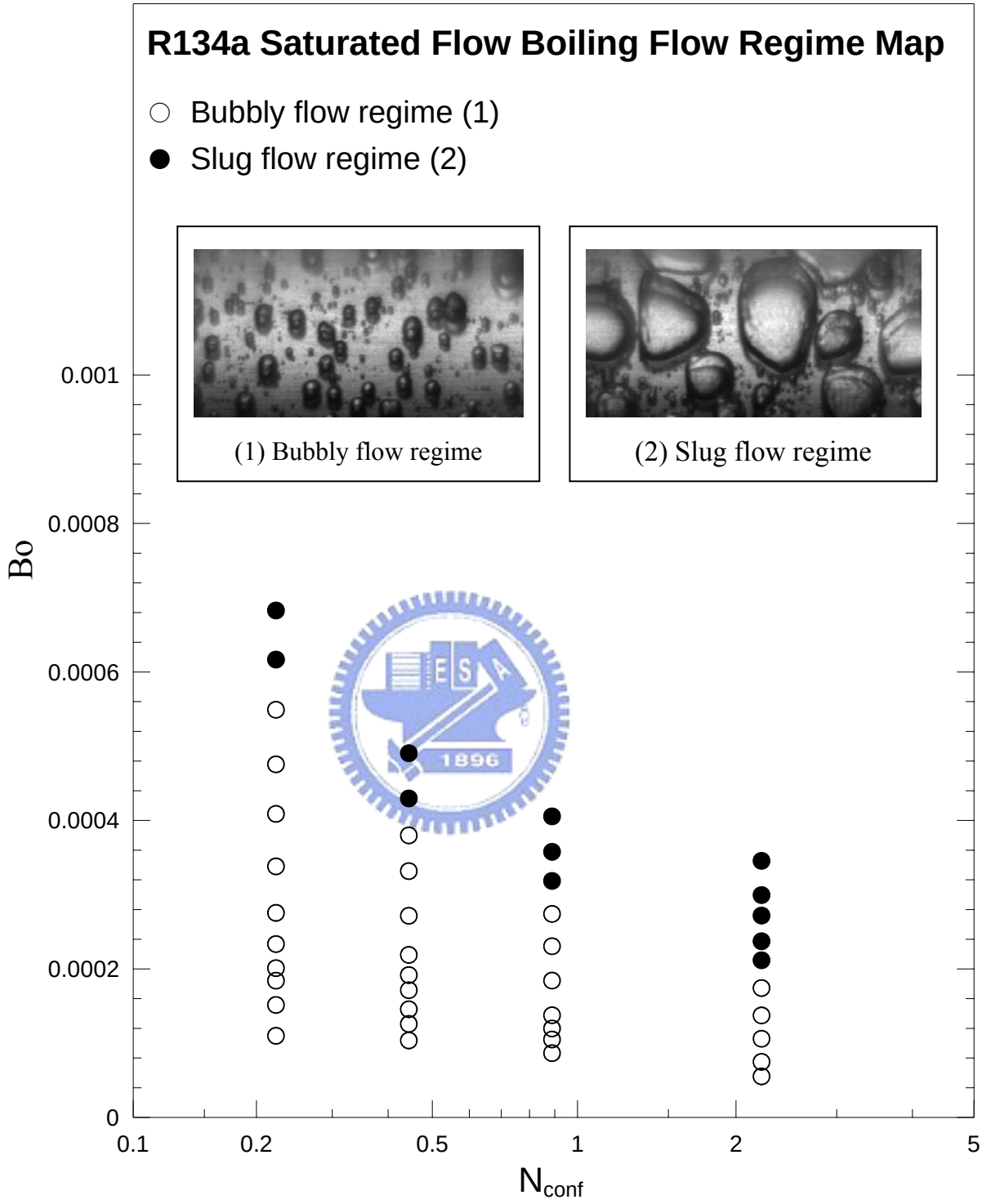

Fig.4.19 Flow regime map for different flow patterns at statistically steady-state observed from flow visualization (43 cases).

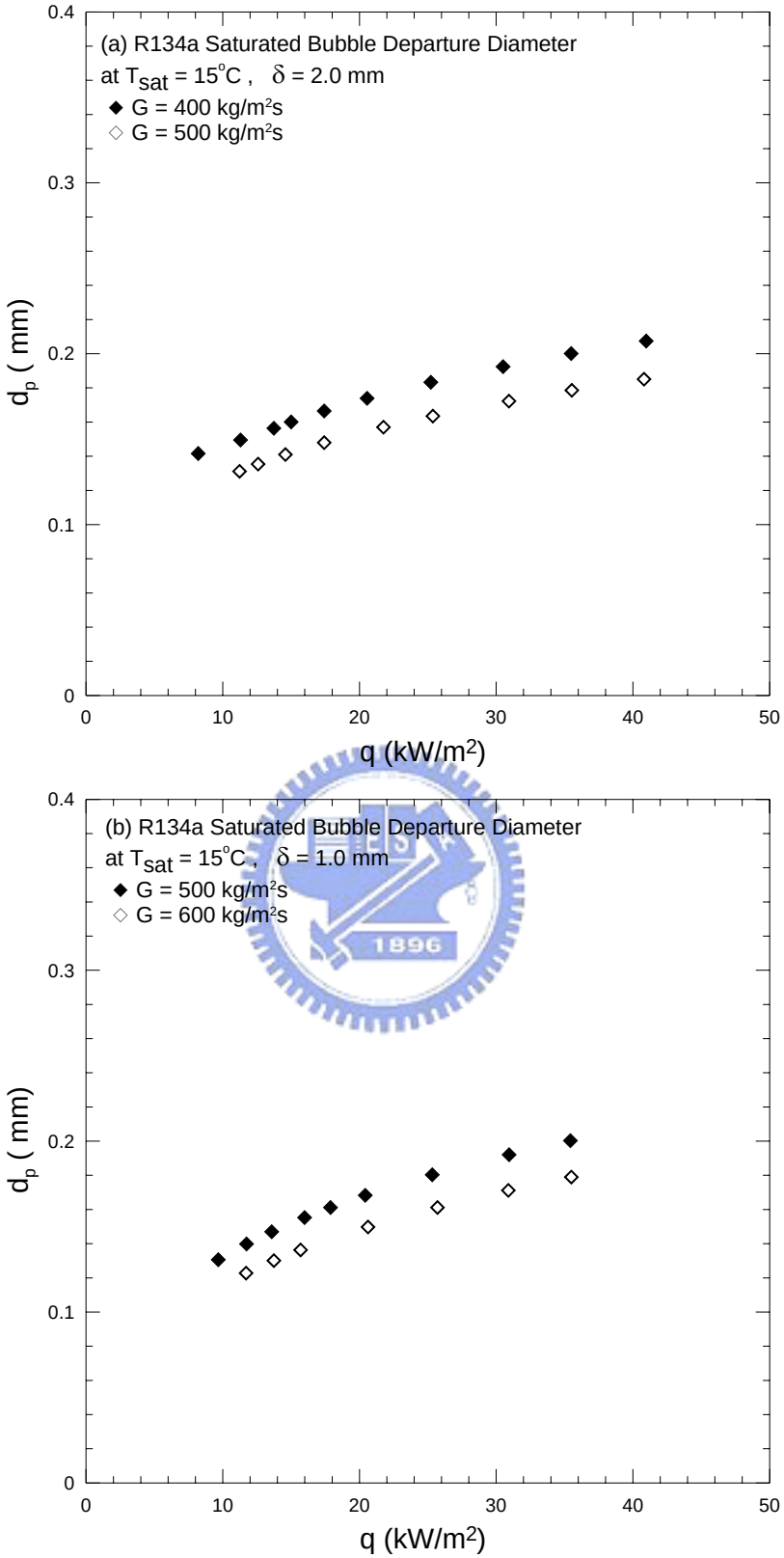

Fig. 4.20 Saturated flow boiling mean bubble departure diameter for various refrigerant mass fluxes at (a) T_{sat}= 15℃ & δ = 2.0 mm and (b) T_{sat}= 15℃ & δ = 1.0 mm.

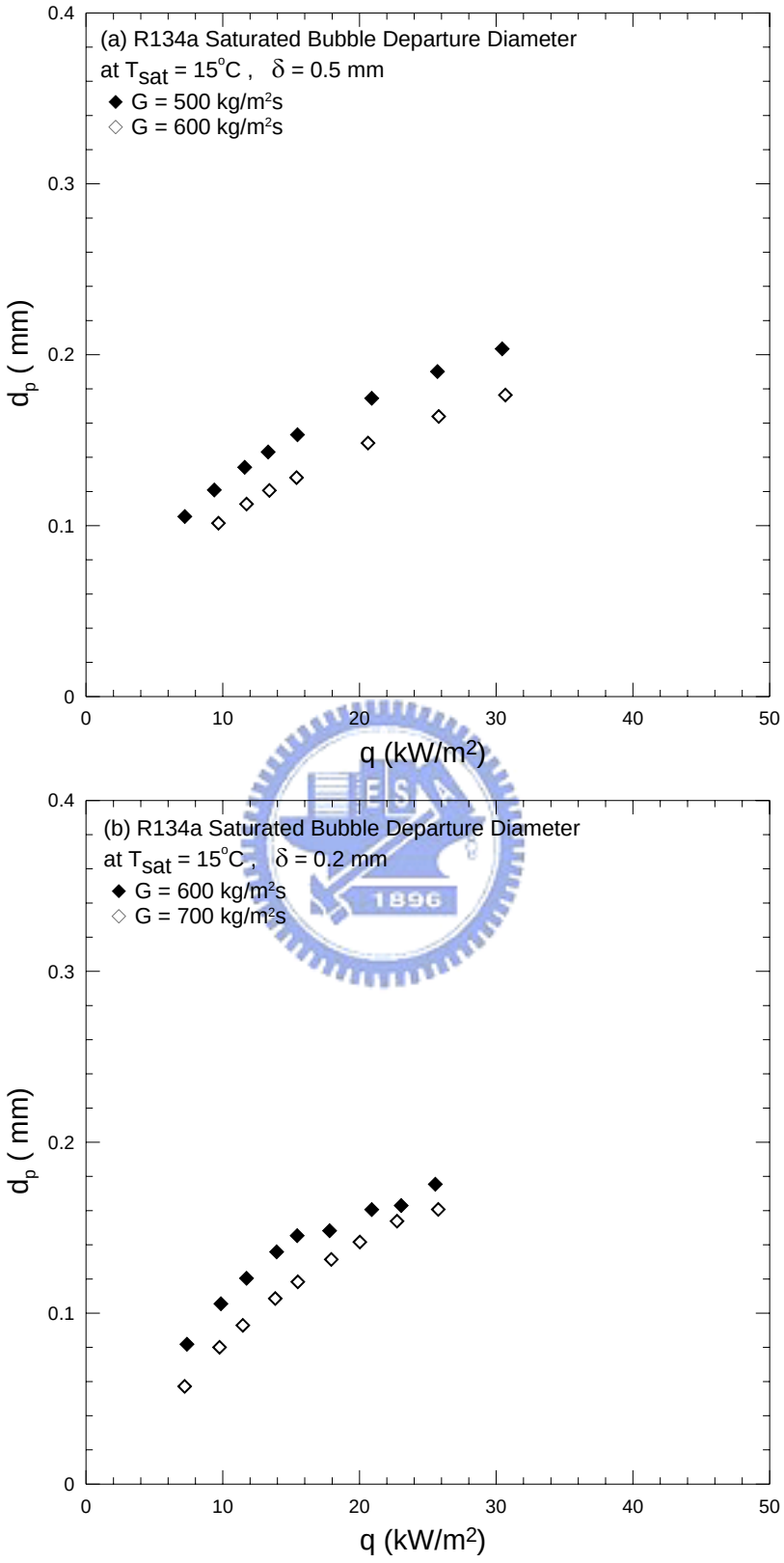

Fig. 4.21 Saturated flow boiling mean bubble departure diameter for various refrigerant mass fluxes at (a) T_{sat}= 15℃ & δ = 0.5 mm and (b) T_{sat}= 15℃ & δ = 0.2 mm.

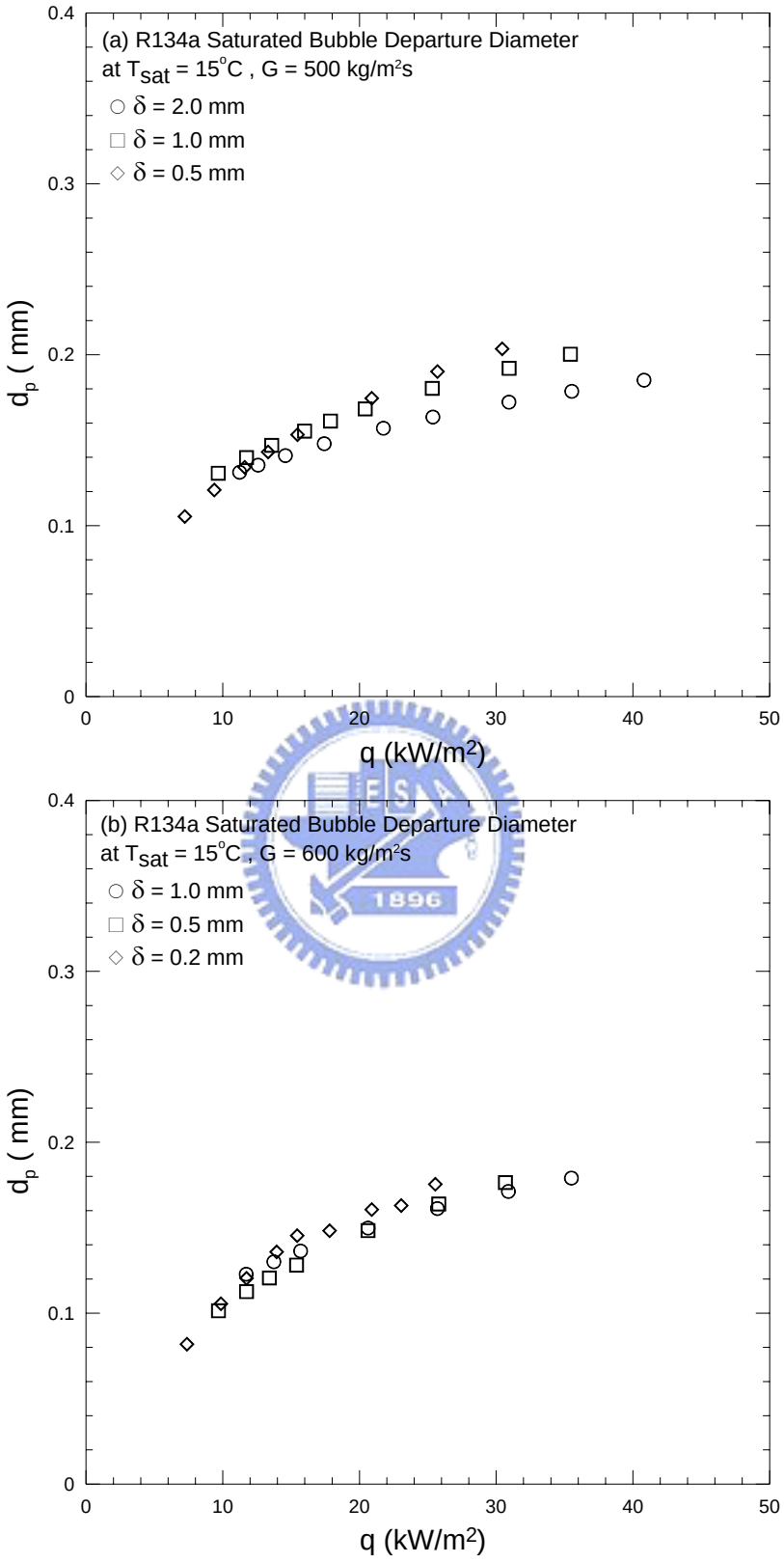

Fig. 4.22 Saturated flow boiling mean bubble departure diameter for various gap sizes at (a) T_{sat}= 15℃ & G= 500 kg/m^{2}s and (b) T_{sat}= 15℃ & G= 600 kg/m^{2}s.

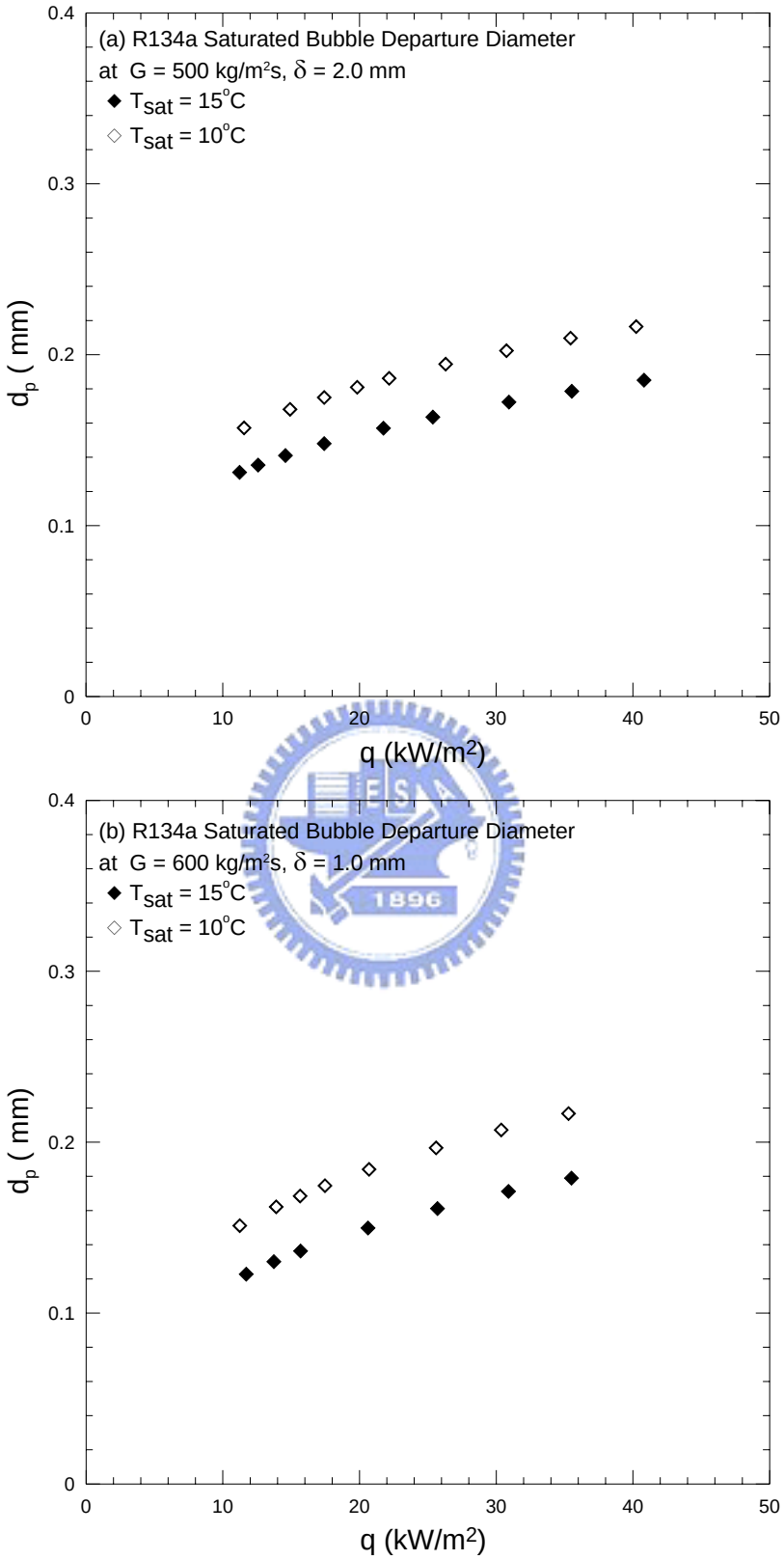

Fig. 4.23 Saturated flow boiling mean bubble departure diameter for various refrigerant saturated temperatures at (a) G= 500 kg/m^{2}s & δ = 2.0 mm and (b) G= 600 kg/m^{2}s & δ = 1.0 mm.

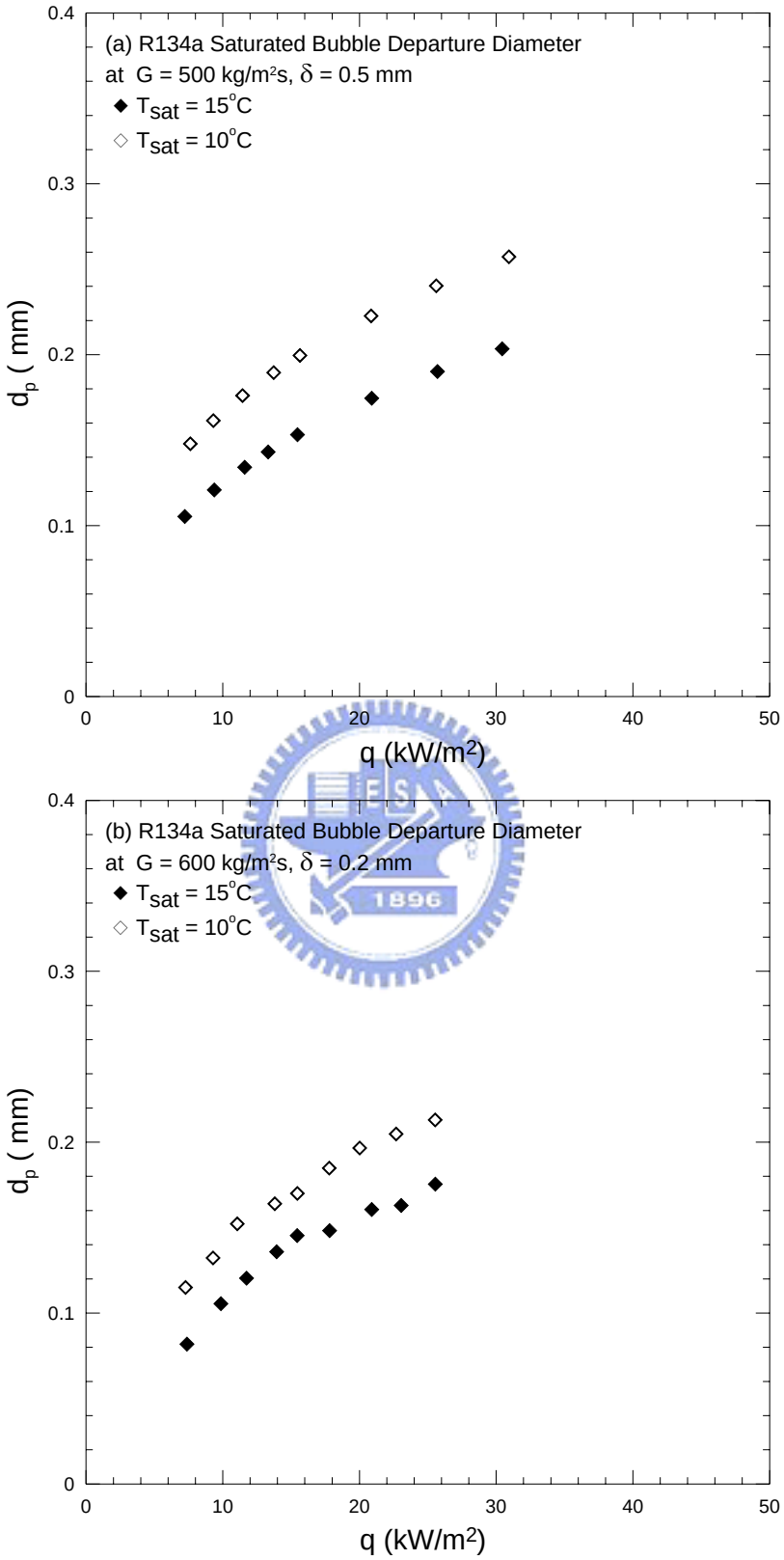

Fig. 4.24 Saturated flow boiling mean bubble departure diameter for various refrigerant saturated temperatures at (a) G= 500 kg/m^{2}s & δ = 0.5 mm and (b) G= 600 kg/m^{2}s & δ = 0.2 mm.

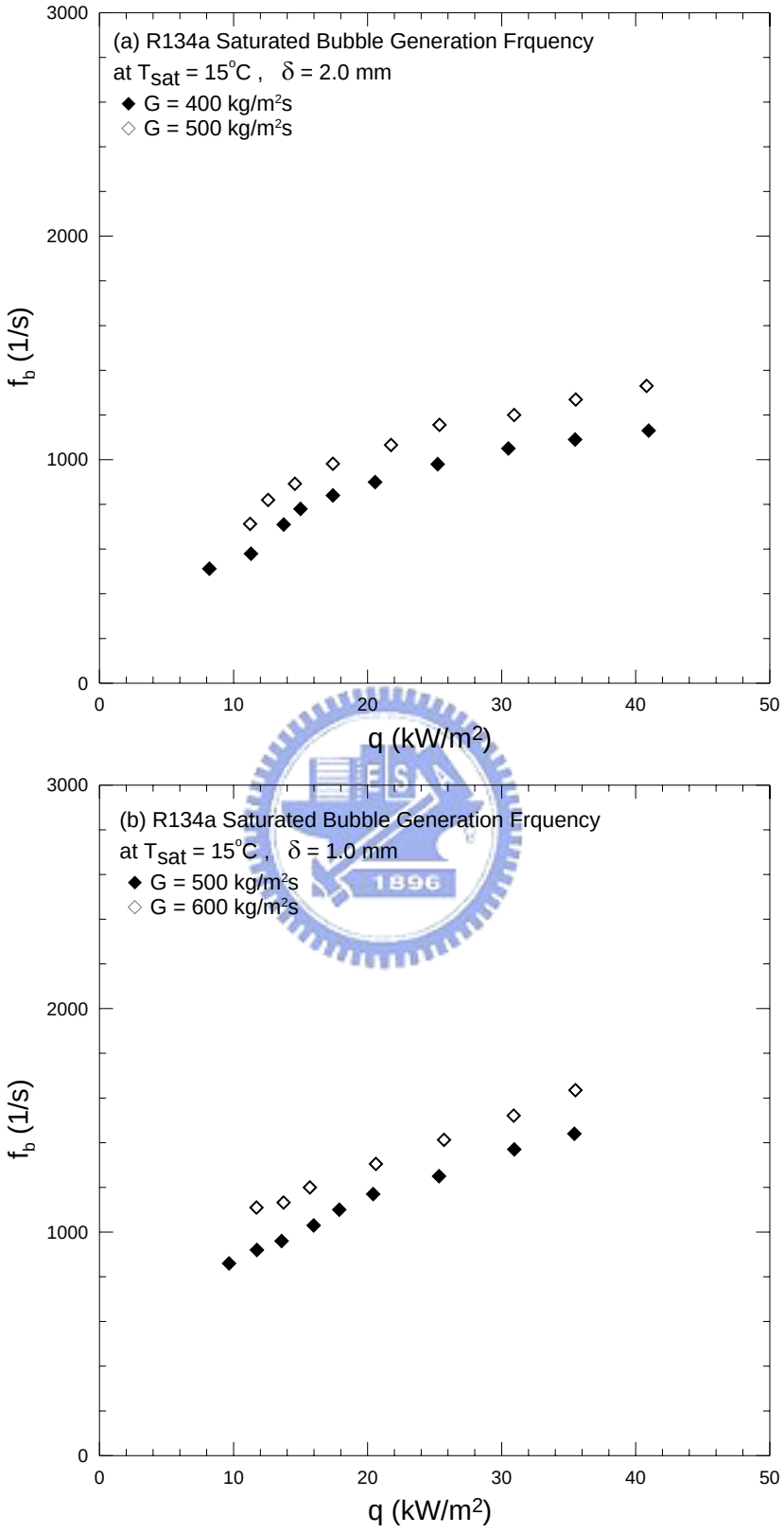

Fig. 4.25 Saturated flow boiling mean bubble departure frequency for various refrigerant mass fluxes at (a) T_{sat}= 15℃ & δ = 2.0 mm and (b) T_{sat}= 15℃ & δ = 1.0 mm.

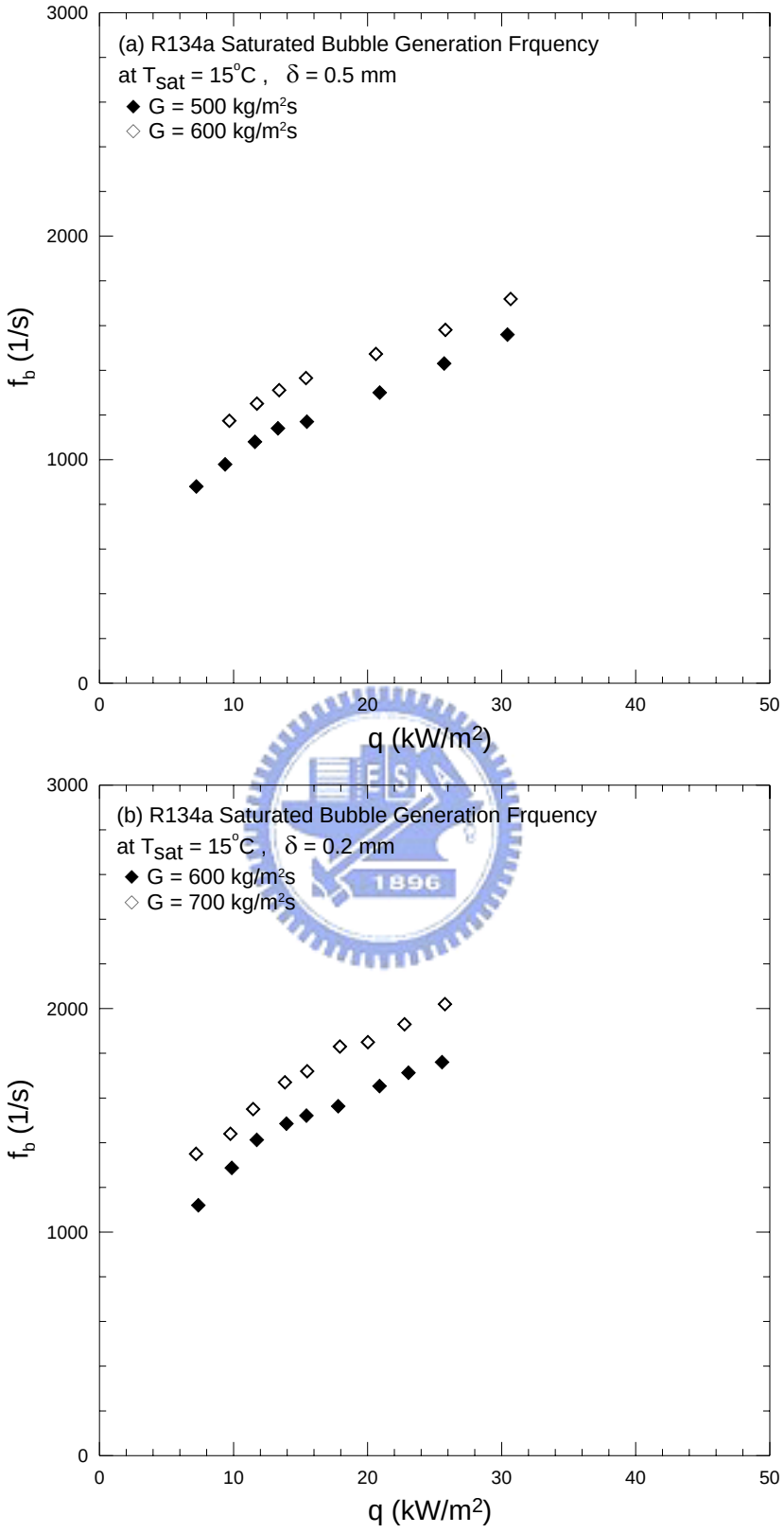

Fig. 4.26 Saturated flow boiling mean bubble departure frequency for various refrigerant mass fluxes at (a) T_{sat}= 15℃ & δ = 0.5 mm and (b) T_{sat}= 15℃ & δ = 0.2 mm.

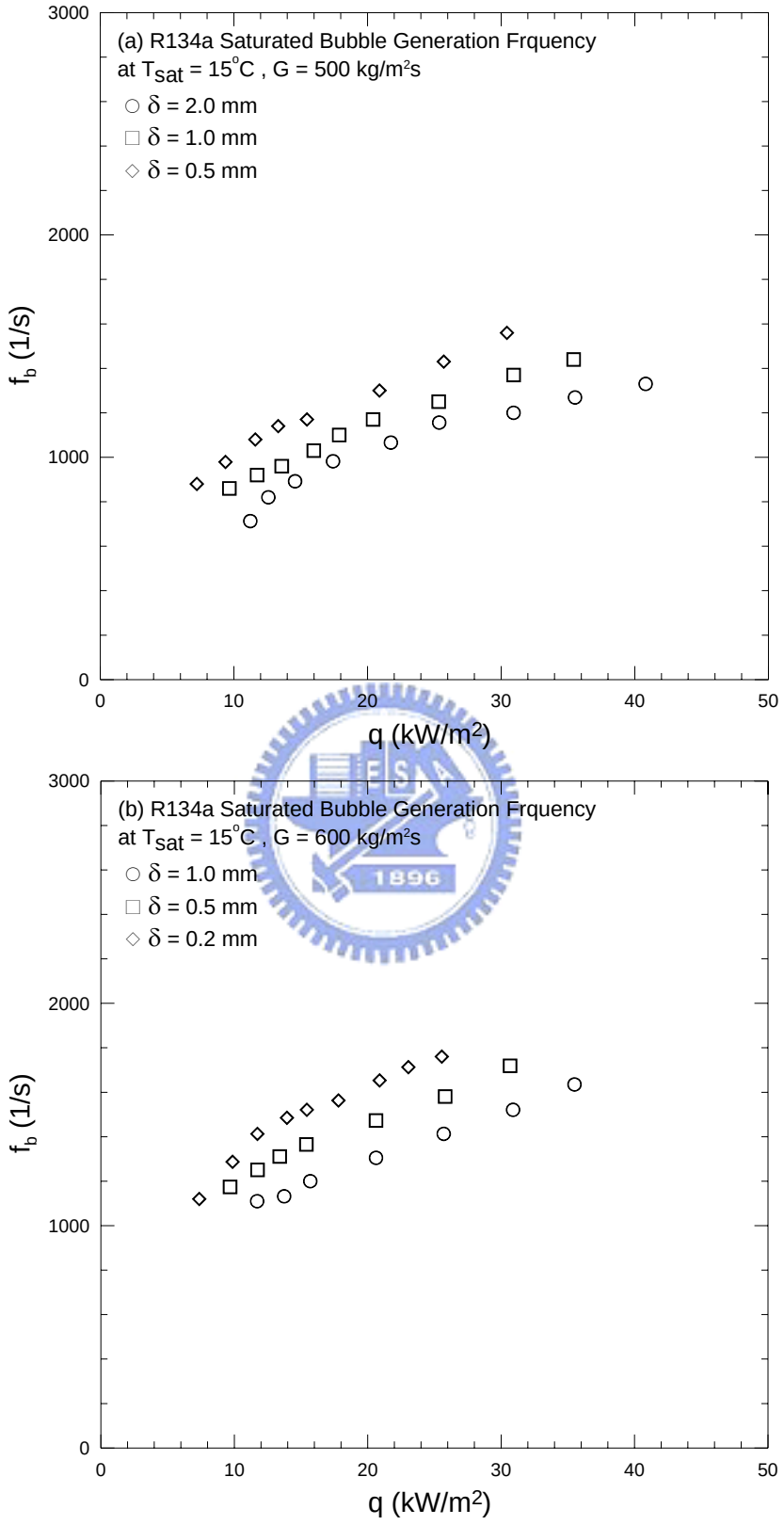

Fig. 4.27 Saturated flow boiling mean bubble departure frequency for various gap sizes at (a) T_{sat}= 15℃ & G= 500 kg/m^{2}s and (b) T_{sat}= 15℃ & G= 600 kg/m^{2}s.

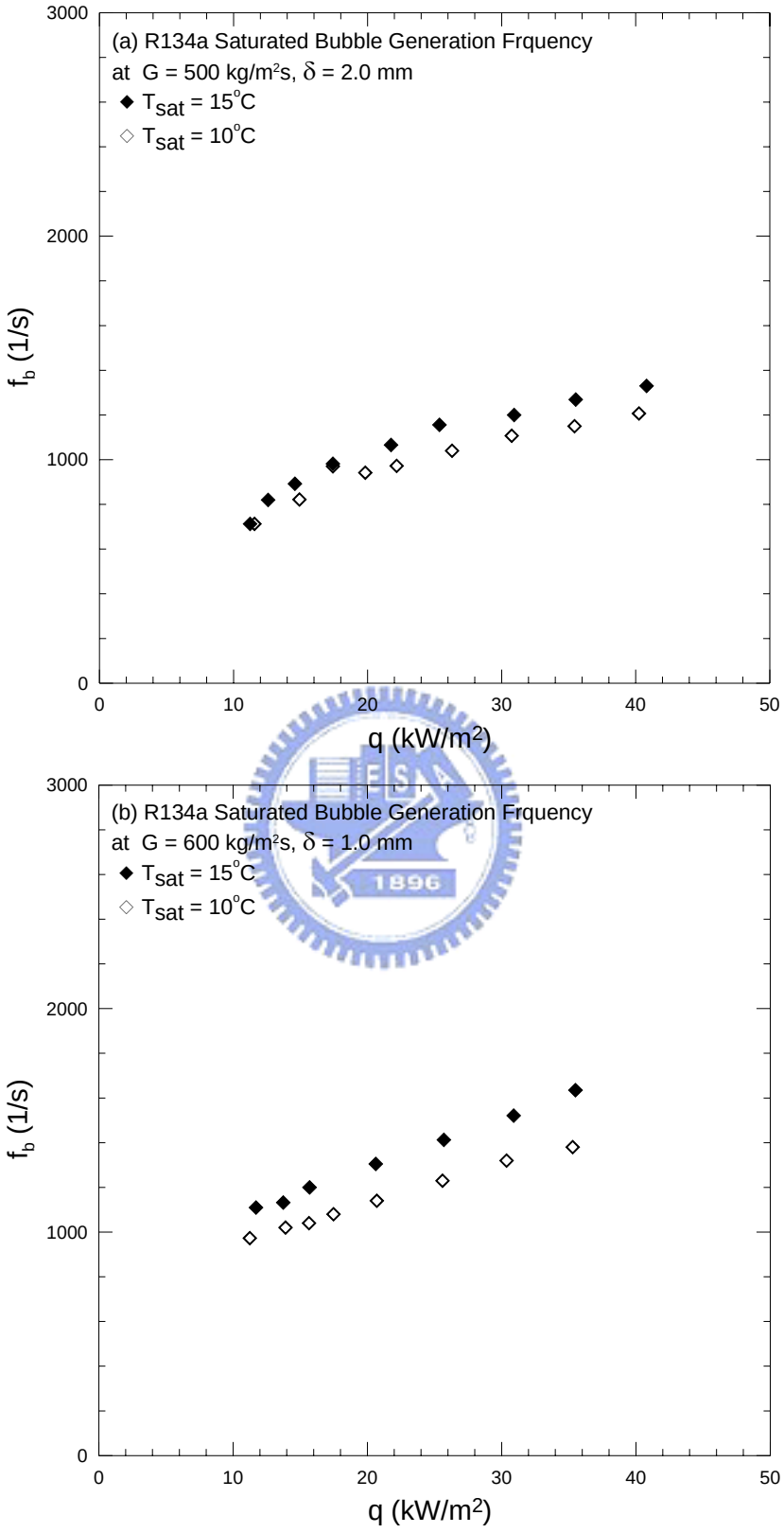

Fig. 4.28 Saturated flow boiling mean bubble departure frequency for various refrigerant saturated temperatures at (a) G= 500 kg/m^{2}s & δ = 2.0 mm and (b) G= 600 kg/m^{2}s & δ = 1.0 mm.

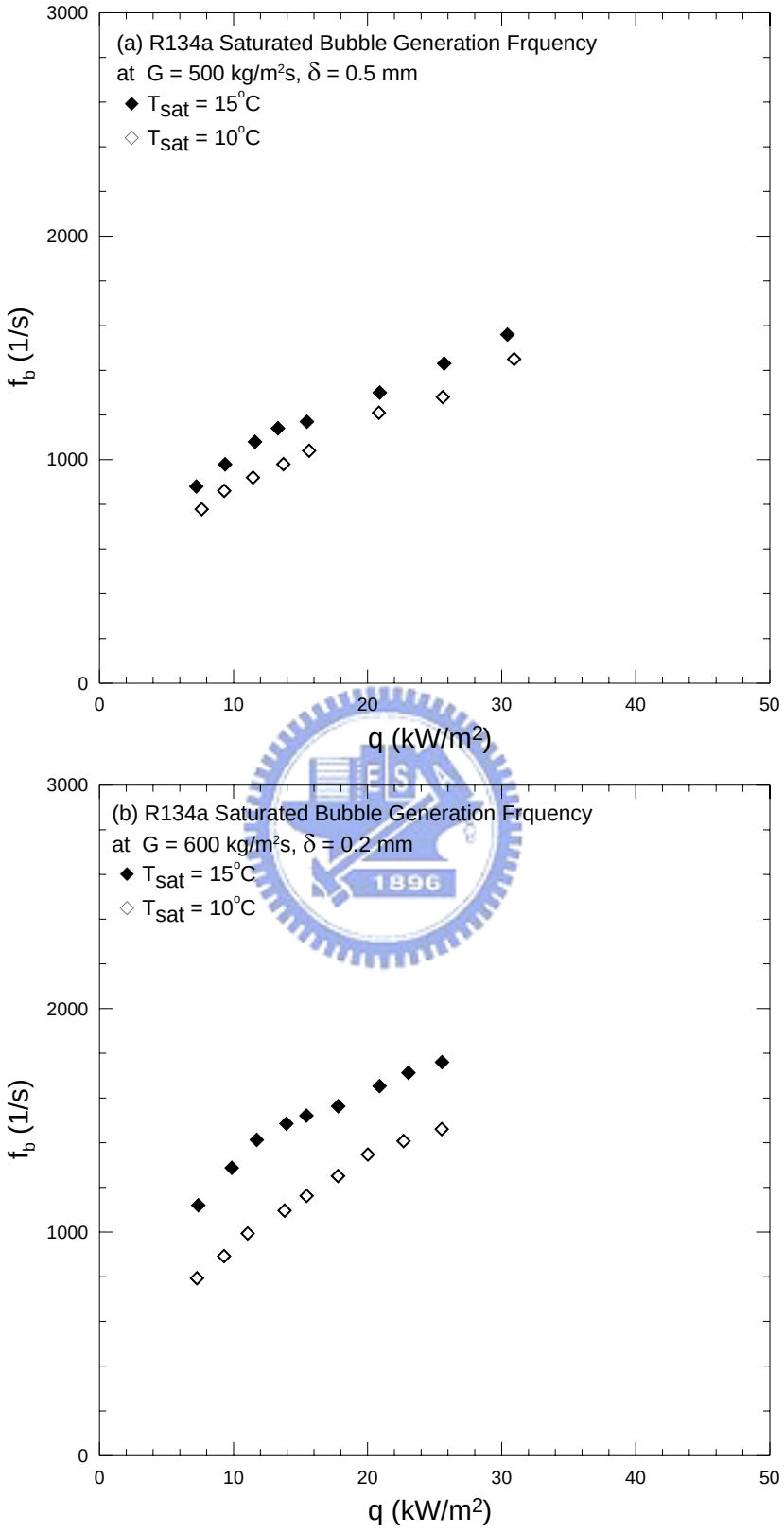

Fig. 4.29 Saturated flow boiling mean bubble departure frequency for various refrigerant saturated temperatures at (a) G= 500 kg/m^{2}s & δ = 0.5 mm and (b) G= 600 kg/m^{2}s & δ = 0.2 mm.

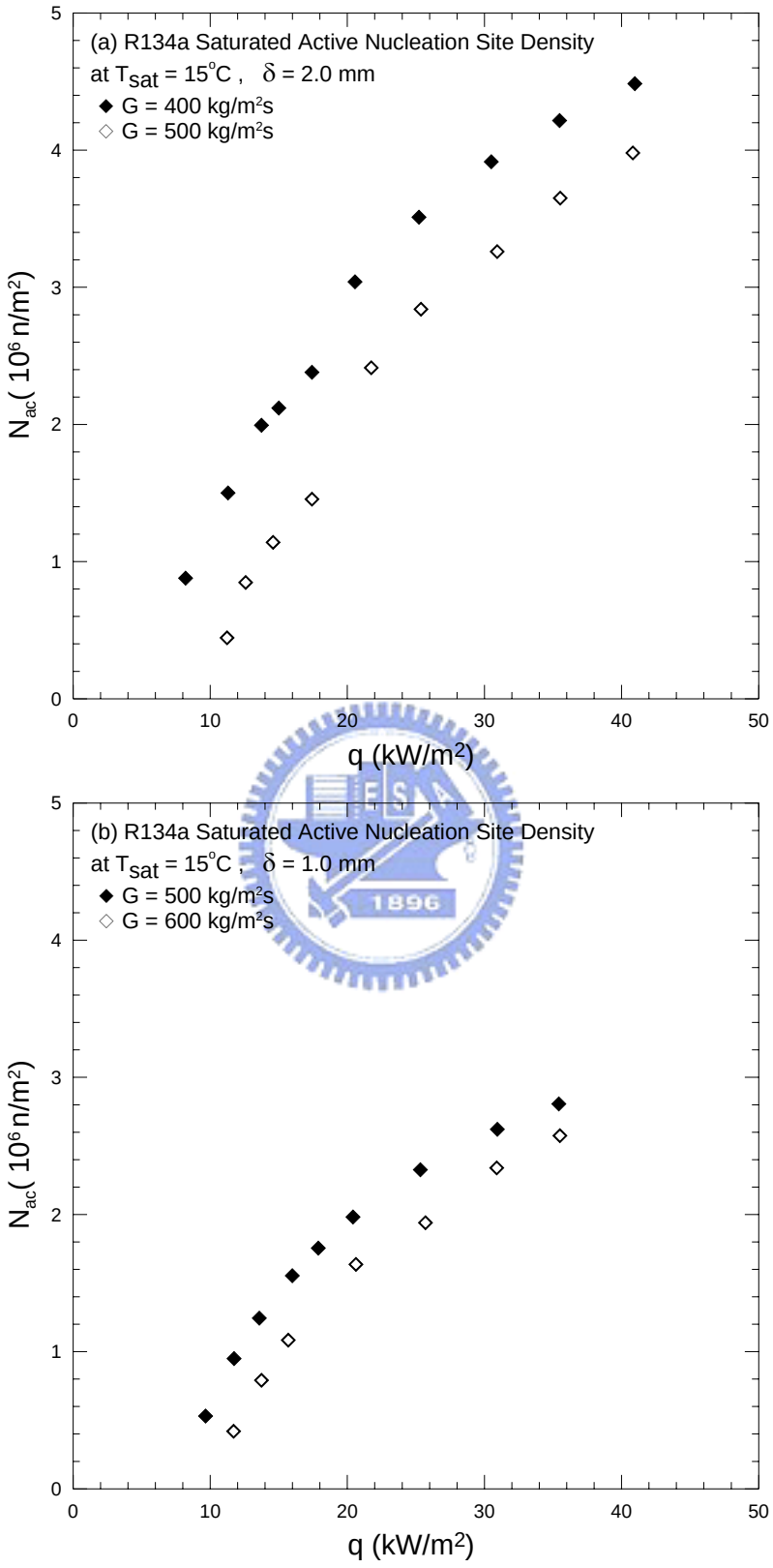

Fig. 4.30 Saturated flow boiling mean active nucleation site density for various refrigerant mass fluxes at (a) T_{sat}= 15℃ & δ = 2.0 mm and (b) T_{sat}= 15℃ & δ = 1.0 mm.

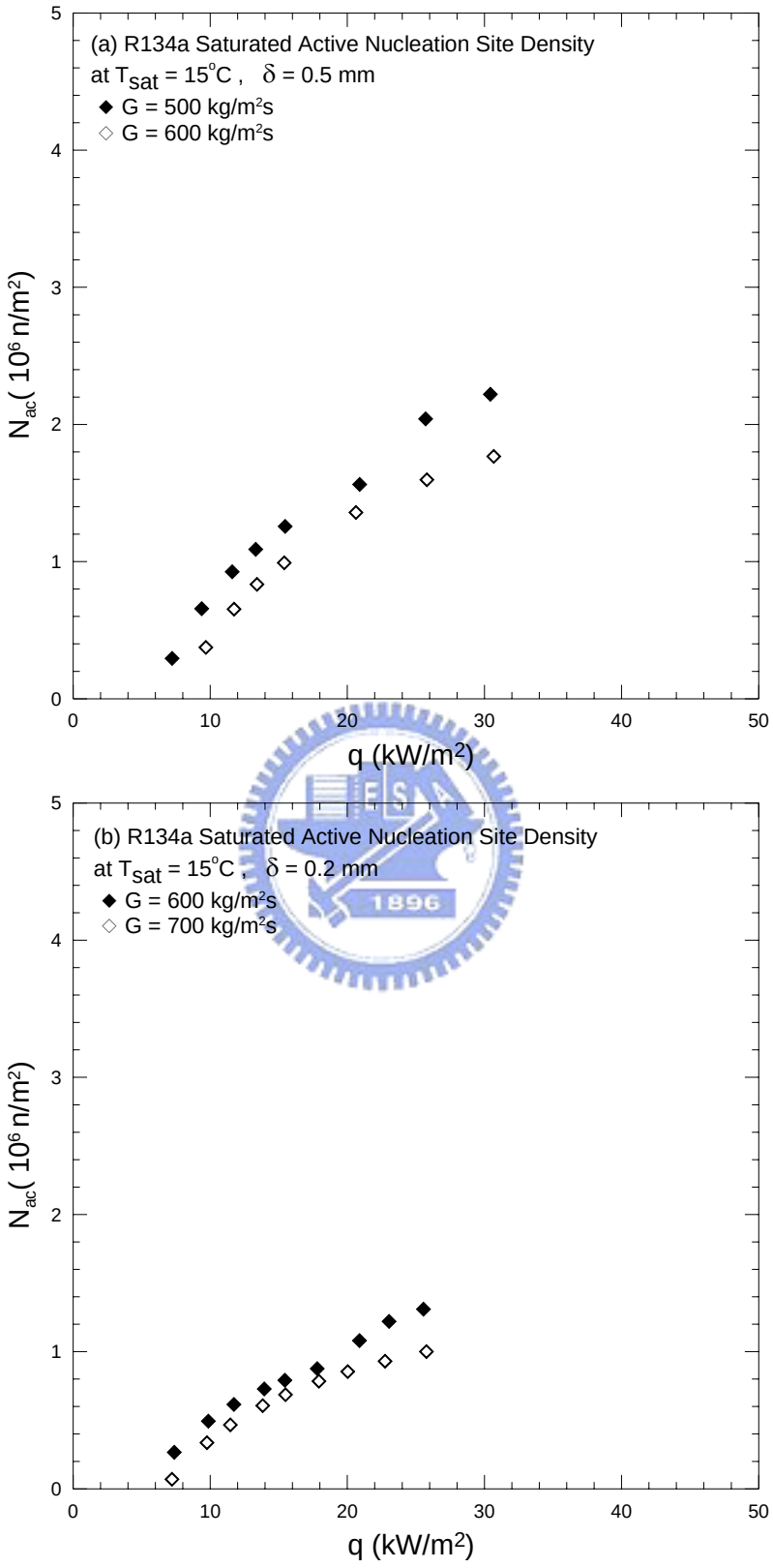

Fig. 4.31 Saturated flow boiling mean active nucleation site density for various refrigerant mass fluxes at (a) T_{sat}= 15℃ & δ = 0.5 mm and (b) T_{sat}= 15℃ & δ = 0.2 mm.

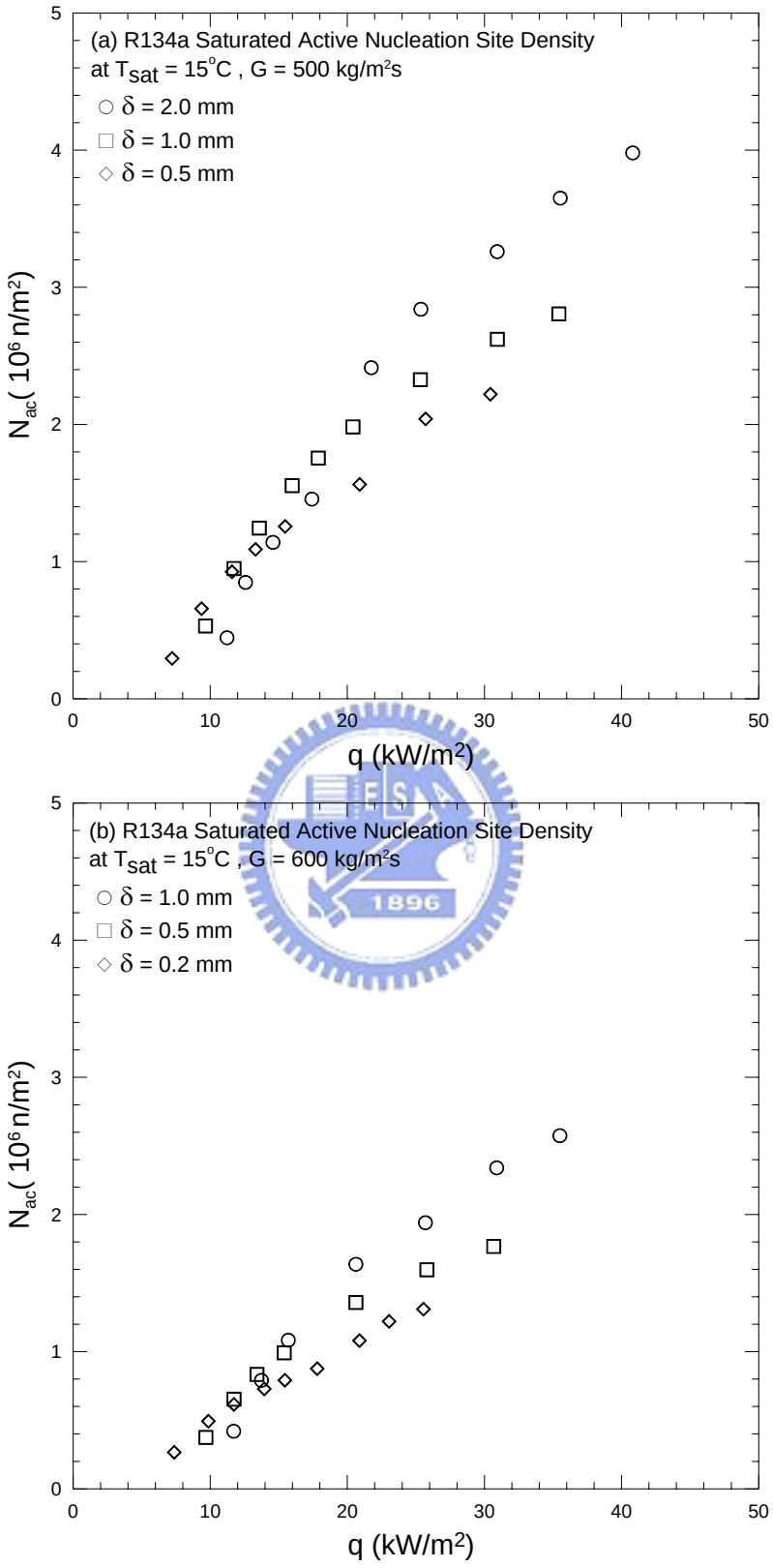

Fig. 4.32 Saturated flow boiling mean active nucleation site density for various gap sizes at (a) T_{sat}= 15℃ & G= 500 kg/m^{2}s and (b) T_{sat}= 15℃ & G= 600 kg/m^{2}s.

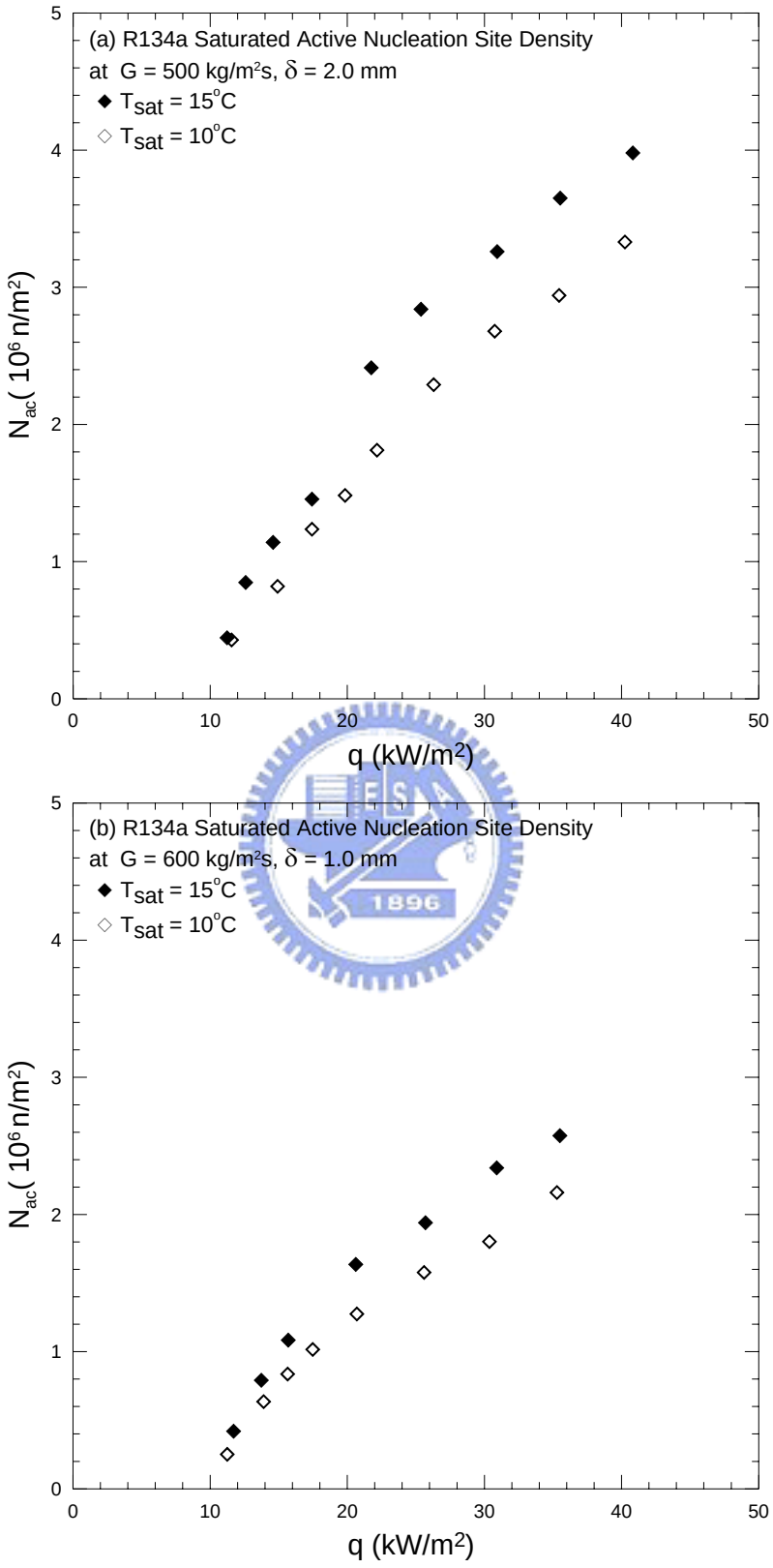

Fig. 4.33 Saturated flow boiling mean active nucleation site density for various refrigerant saturated temperatures at (a) G= 500 kg/m^{2}s & δ = 2.0 mm and (b) G= 600 kg/m^{2}s & δ = 1.0 mm.

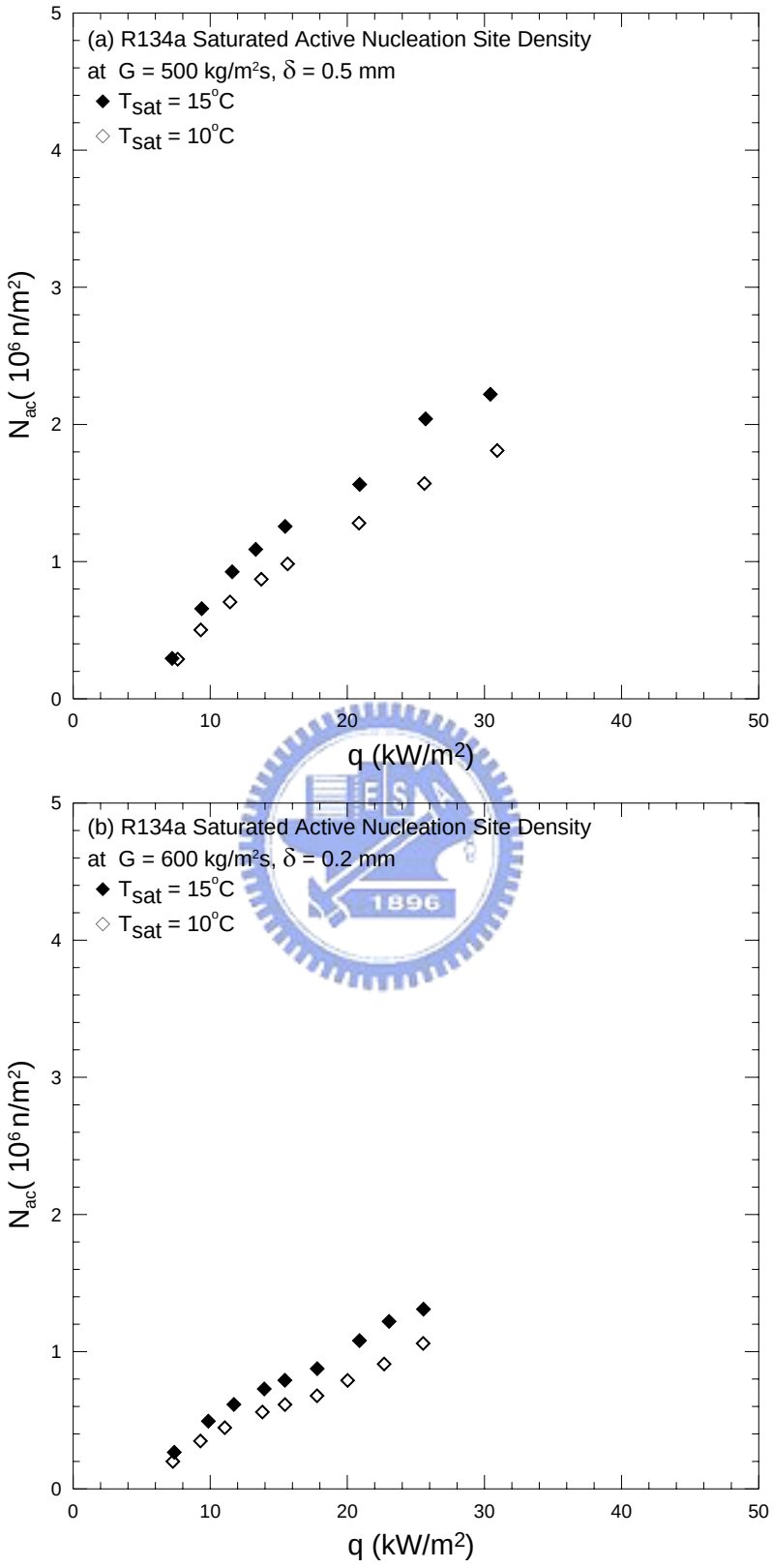

Fig. 4.34 Saturated flow boiling mean active nucleation site density for various refrigerant saturated temperatures at (a) G= 500 kg/m^{2}s & δ = 0.5 mm and (b) G= 600 kg/m^{2}s & δ = 0.2 mm.

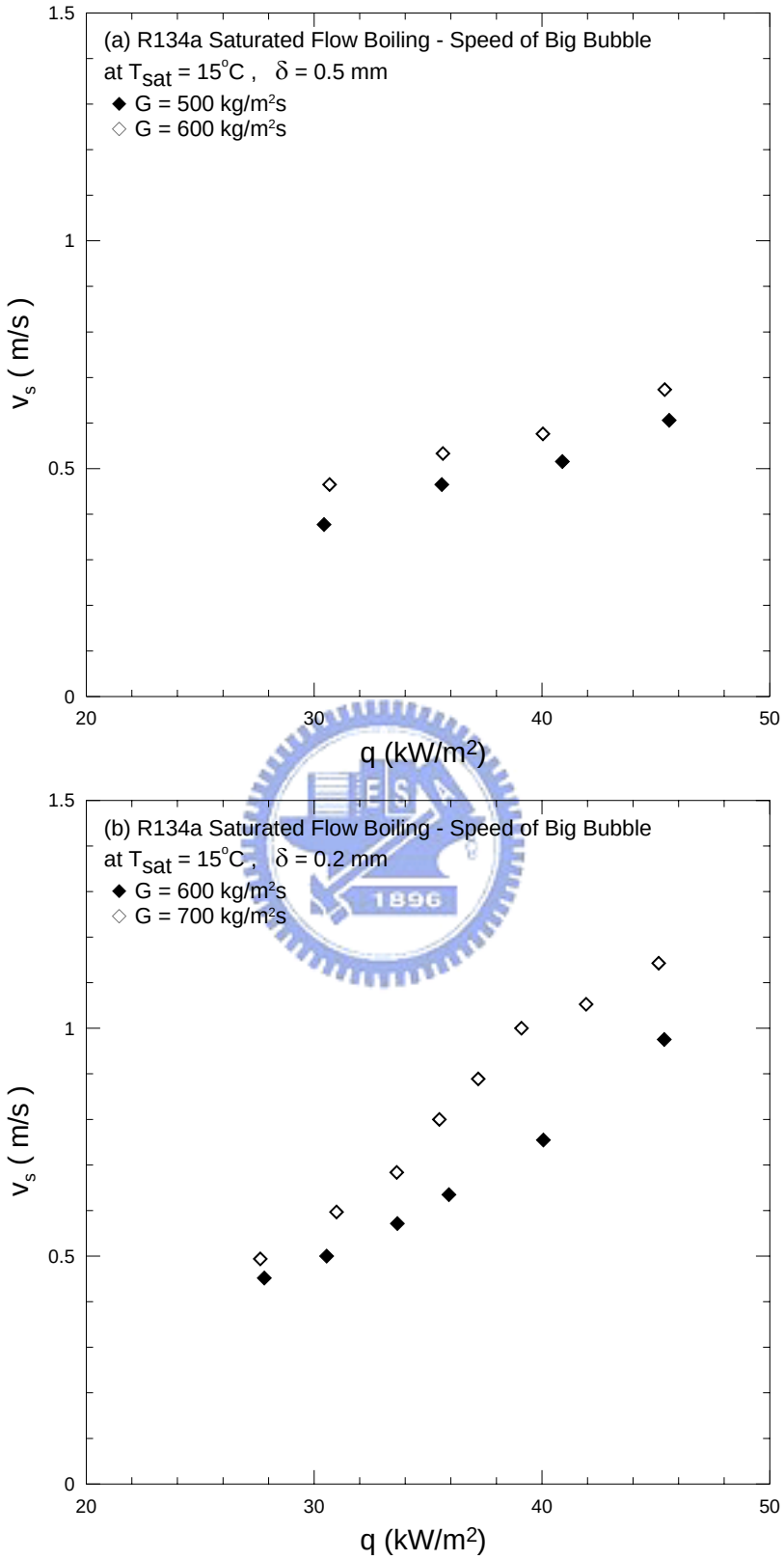

Fig. 4.35 Mean axial speed of the big bubbles in slug flow for various refrigerant mass fluxes at (a) T_{sat}= 15℃ & δ = 0.5 mm and (b) T_{sat}= 15℃ & δ = 0.2 mm.

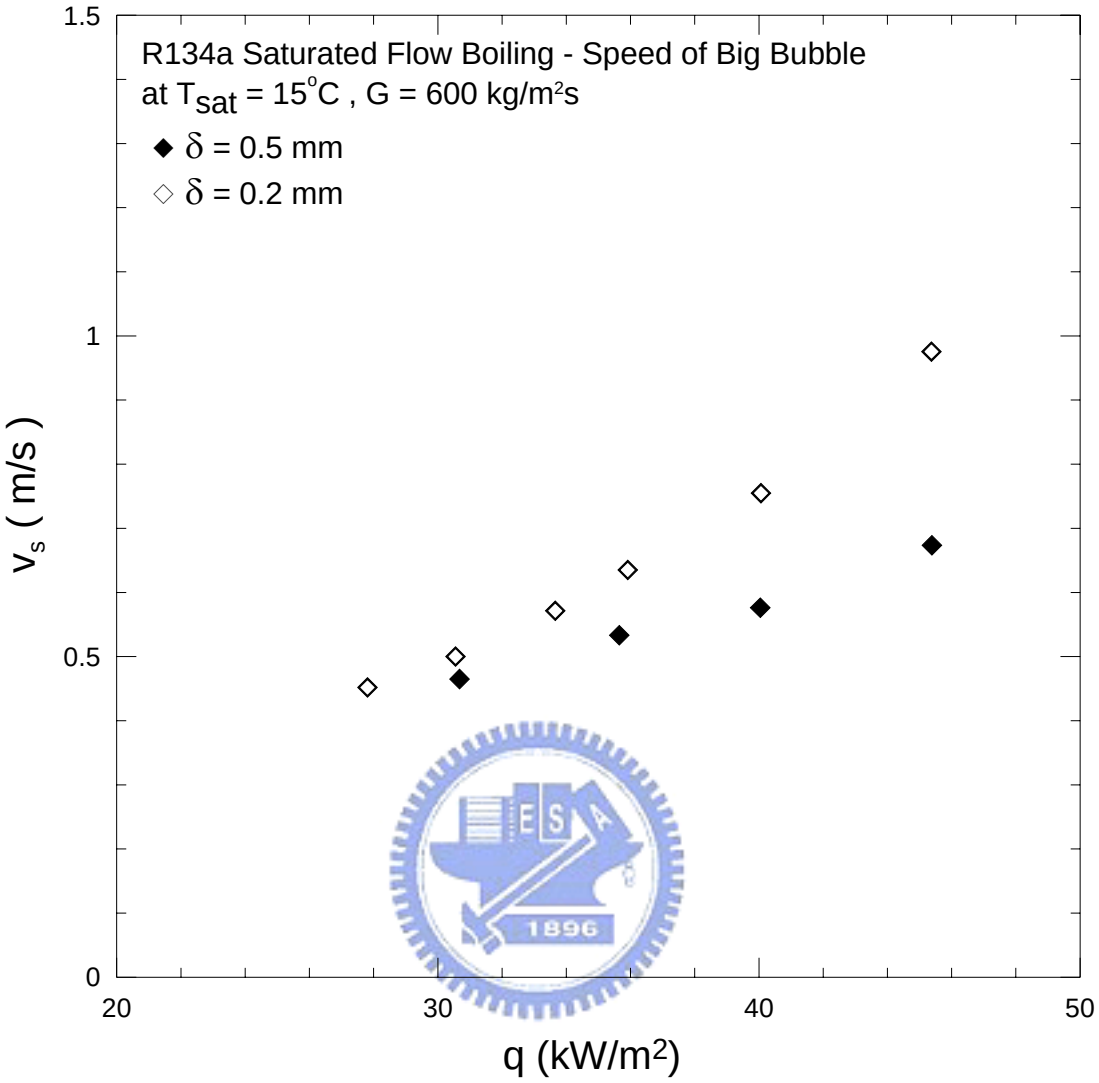

Fig. 4.36 Mean axial speed of the big bubbles in slug flow for various gap sizes at T_{sat}= 15℃ & G= 600 kg/m^2s.

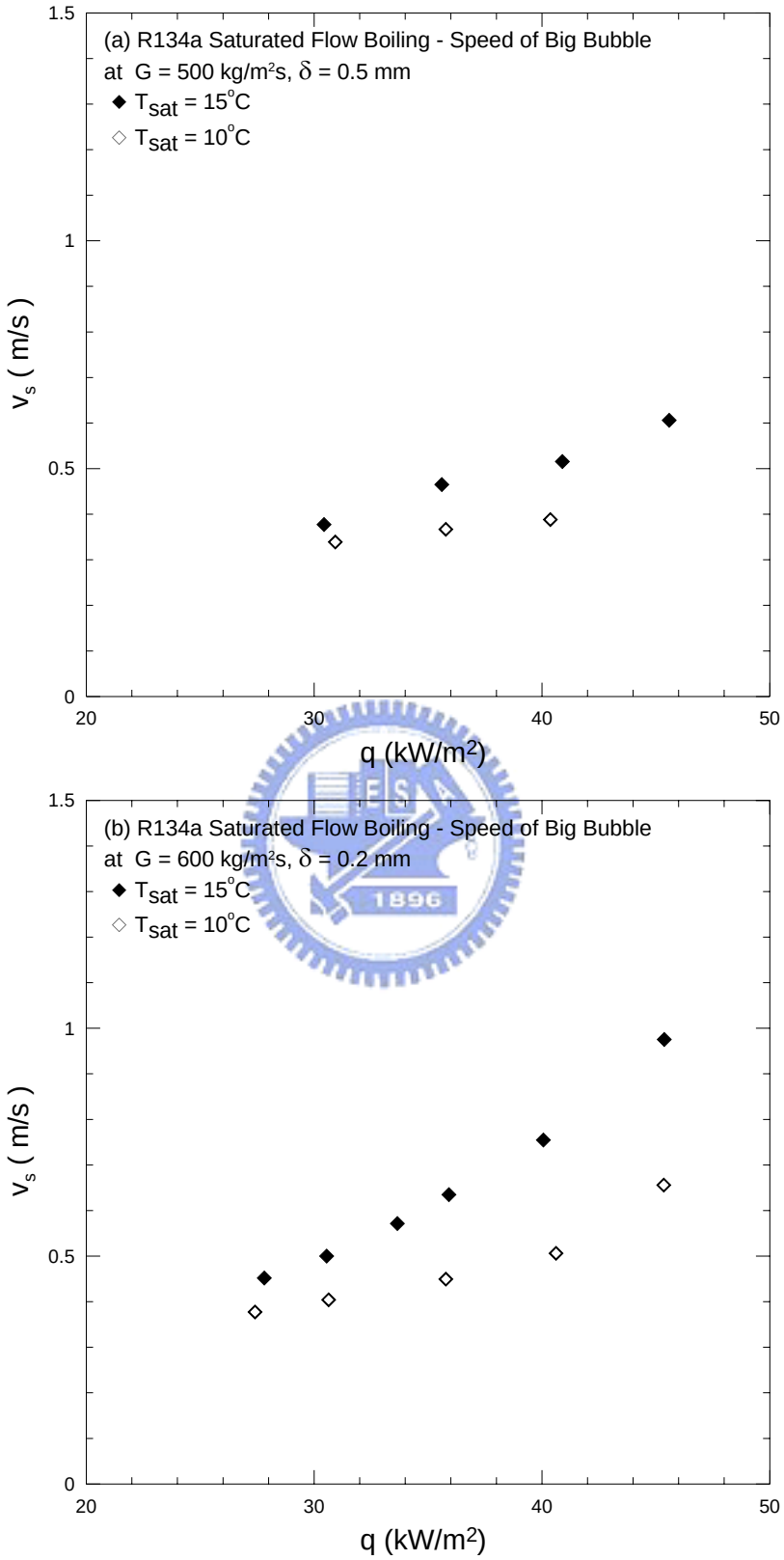

Fig. 4.37 Mean axial speed of the big bubbles in slug flow for various refrigerant saturated temperatures at (a) G= 500 kg/m^{2}s & δ = 0.5 mm and (b) G= 600 kg/m^{2}s & δ = 0.2 mm.

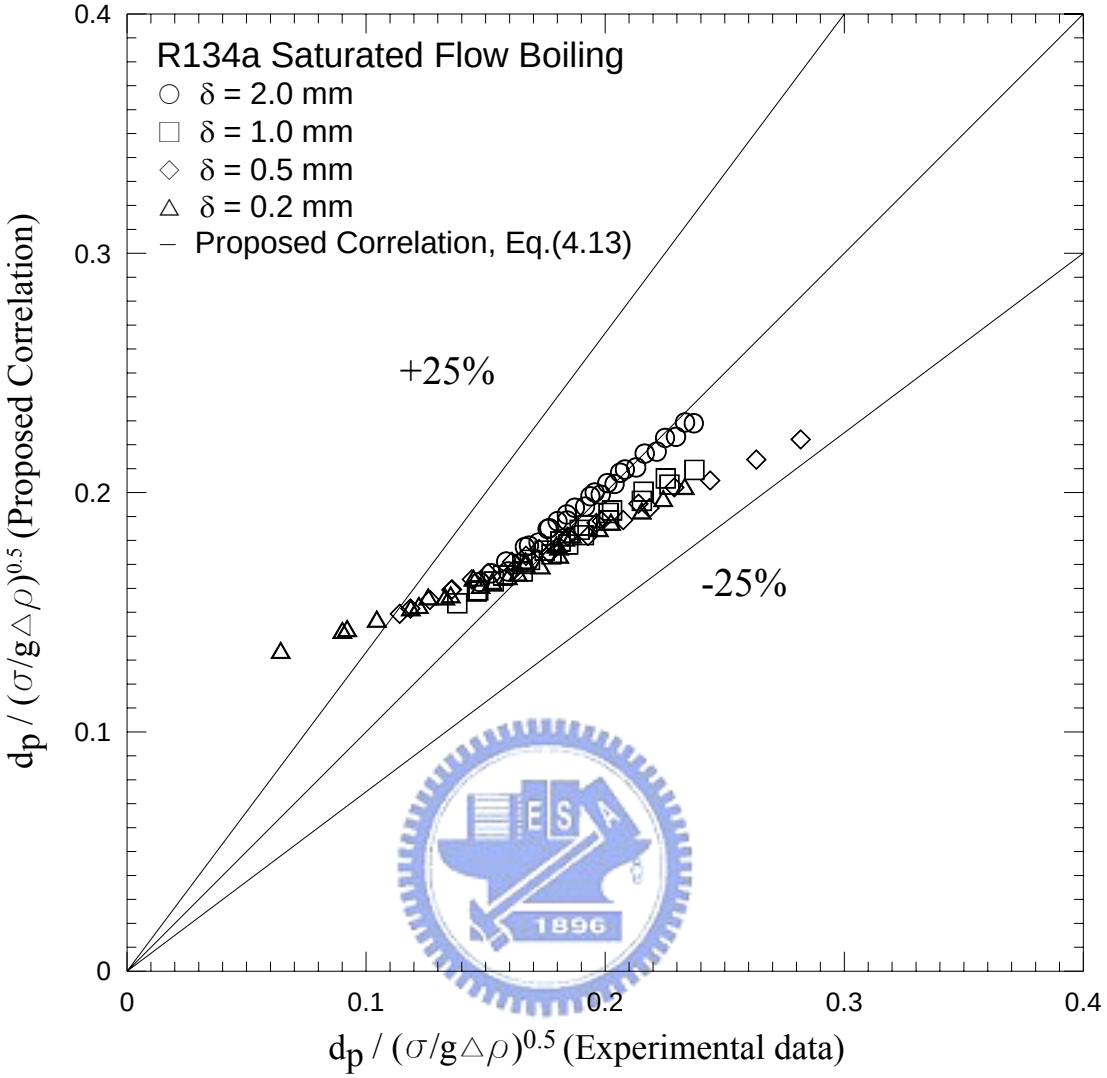

Fig. 4.38 Comparison of the measured data for mean bubble departure diameter in the saturated flow boiling of R-134a with the proposed correlation.

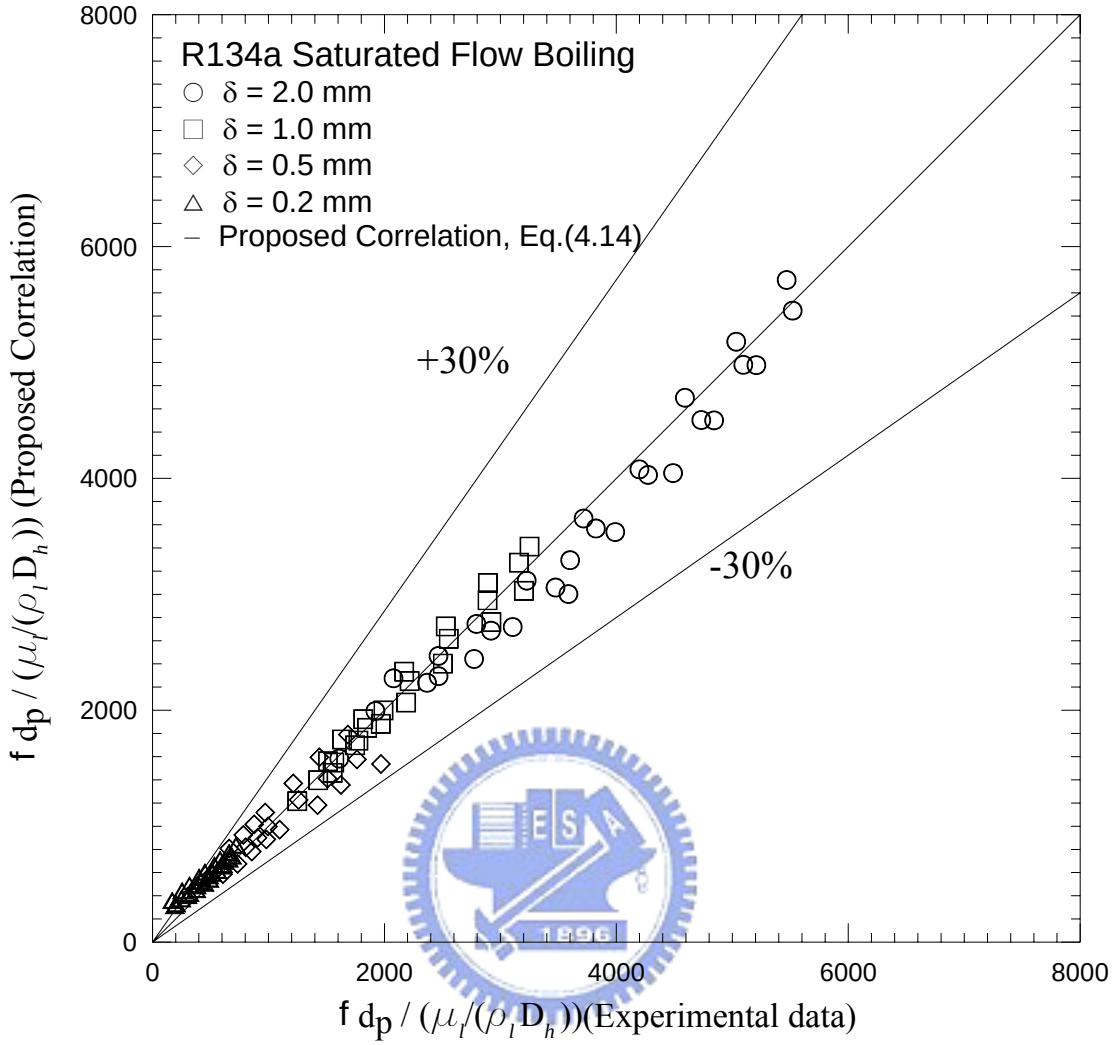

Fig. 4.39 Comparison of the measured data for mean bubble departure frequency in the saturated flow boiling of R-134a with the proposed correlation.

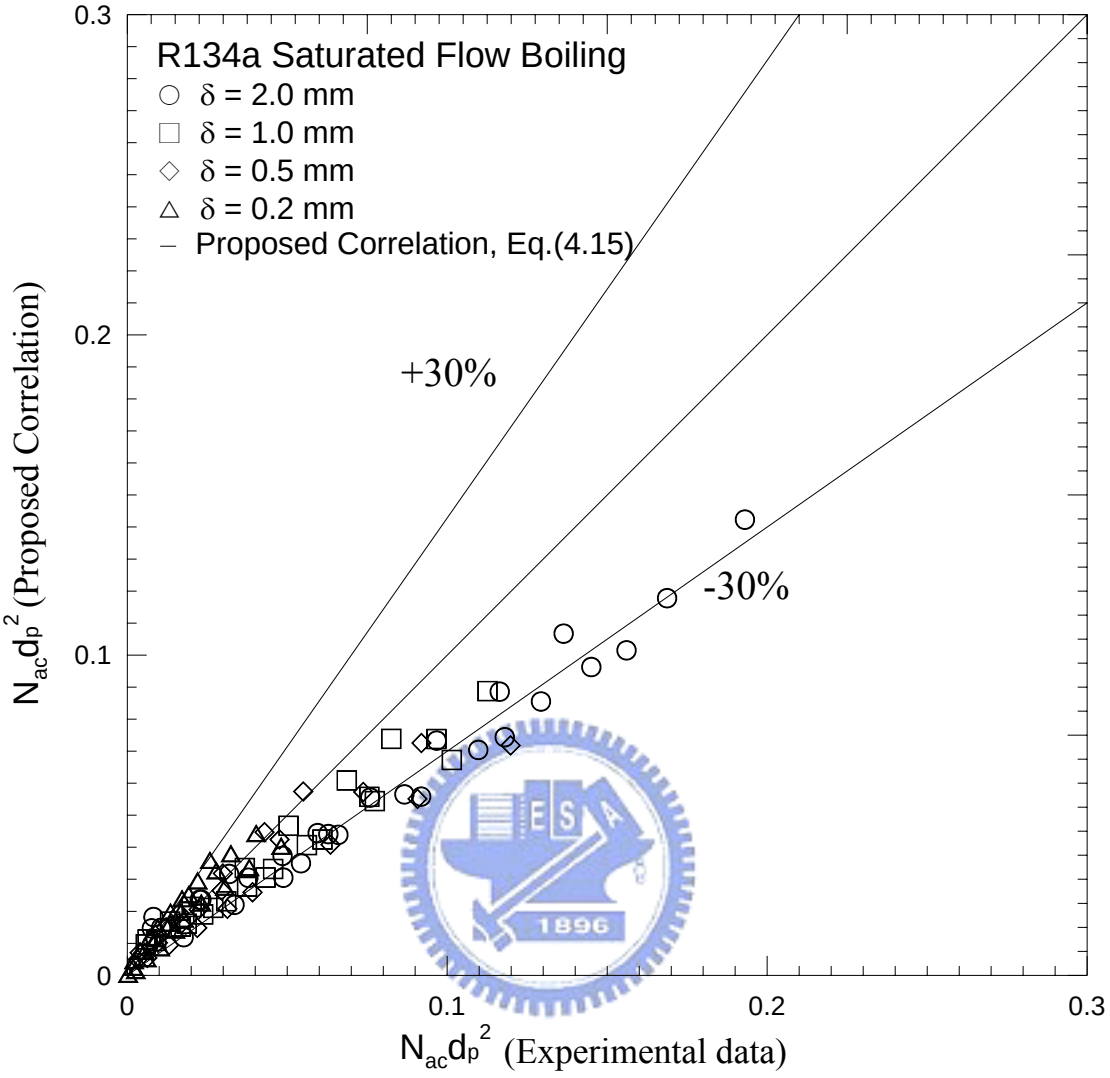

Fig. 4.40 Comparison of the measured data for mean active nucleation site density in the saturated flow boiling of R-134a with the proposed correlation.

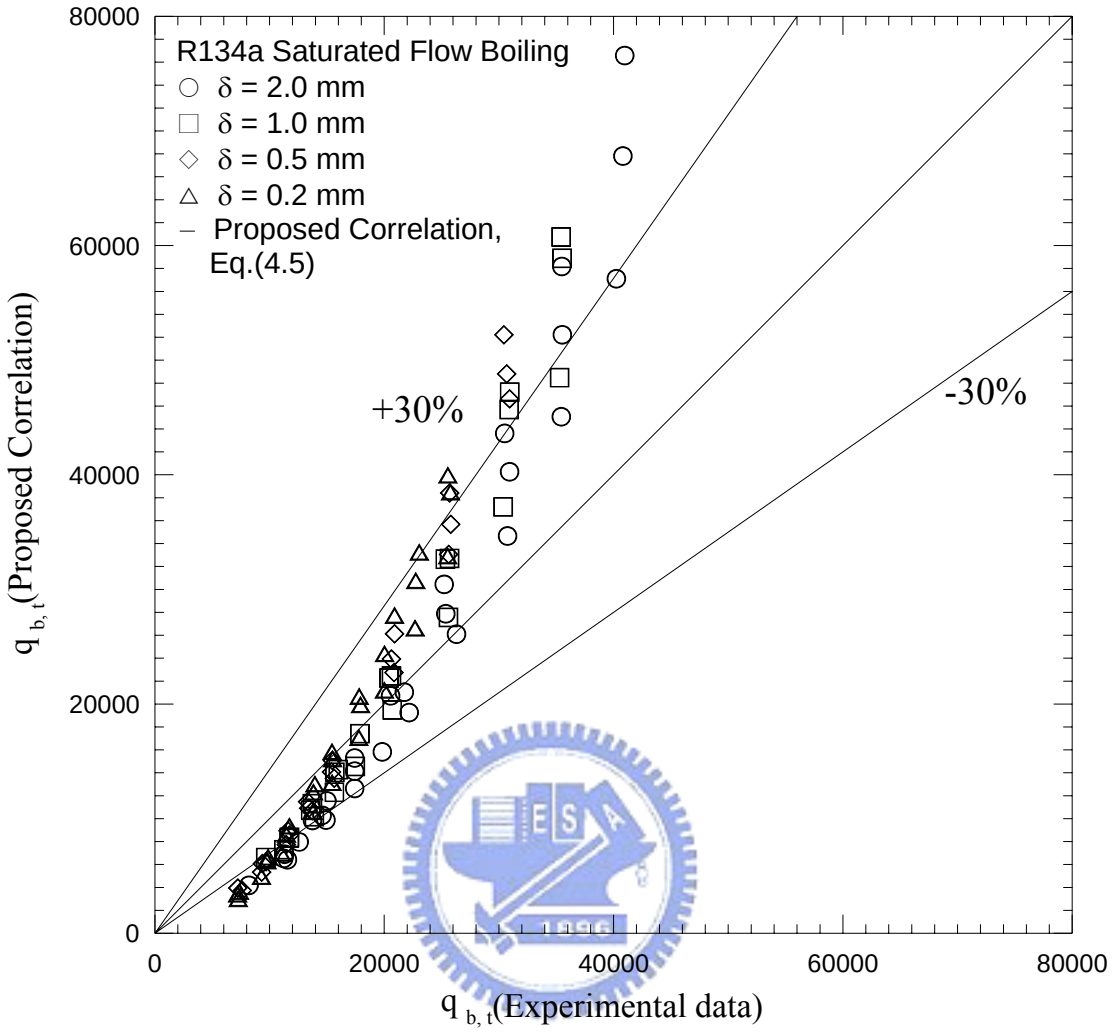

Fig. 4.41 Comparison of the measured data for heat transfer coefficient in the saturated flow boiling of R-134a in the bubbly flow regime with the proposed correlation.

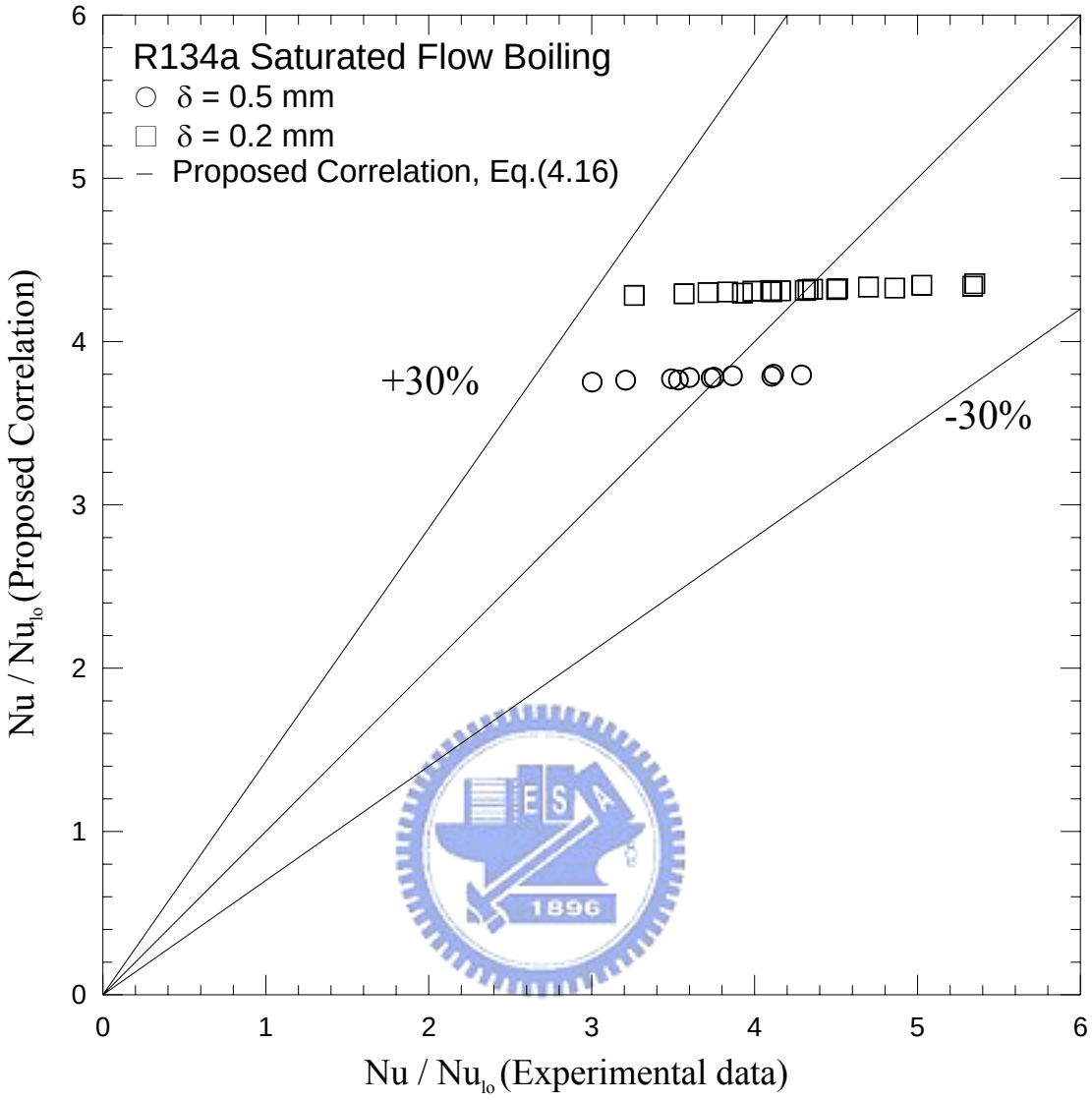

Fig. 4.42 Comparison of the measured data for heat transfer coefficient in the saturated flow boiling of R-134a in the slug flow regime with the proposed correlation.